NASA/TM—2020-220380

Durability of YSZ Coated Ti_2AlC in 1300 °C Mach 0.3 Burner Rig Tests

James L. Smialek
Glenn Research Center, Cleveland, Ohio

Michael D. Cuy
Vantage Partners, LLC, Brook Park, Ohio

Bryan J. Harder
Glenn Research Center, Cleveland, Ohio

Anita Garg
The University of Toledo, Toledo, Ohio

Richard B. Rogers
Glenn Research Center, Cleveland, Ohio

February 2020

NASA STI Program . . . in Profile

Since its founding, NASA has been dedicated to the advancement of aeronautics and space science. The NASA Scientific and Technical Information (STI) Program plays a key part in helping NASA maintain this important role.

The NASA STI Program operates under the auspices of the Agency Chief Information Officer. It collects, organizes, provides for archiving, and disseminates NASA's STI. The NASA STI Program provides access to the NASA Technical Report Server—Registered (NTRS Reg) and NASA Technical Report Server—Public (NTRS) thus providing one of the largest collections of aeronautical and space science STI in the world. Results are published in both non-NASA channels and by NASA in the NASA STI Report Series, which includes the following report types:

- TECHNICAL PUBLICATION. Reports of completed research or a major significant phase of research that present the results of NASA programs and include extensive data or theoretical analysis. Includes compilations of significant scientific and technical data and information deemed to be of continuing reference value. NASA counter-part of peer-reviewed formal professional papers, but has less stringent limitations on manuscript length and extent of graphic presentations.

- TECHNICAL MEMORANDUM. Scientific and technical findings that are preliminary or of specialized interest, e.g., "quick-release" reports, working papers, and bibliographies that contain minimal annotation. Does not contain extensive analysis.

- CONTRACTOR REPORT. Scientific and technical findings by NASA-sponsored contractors and grantees.

- CONFERENCE PUBLICATION. Collected papers from scientific and technical conferences, symposia, seminars, or other meetings sponsored or co-sponsored by NASA.

- SPECIAL PUBLICATION. Scientific, technical, or historical information from NASA programs, projects, and missions, often concerned with subjects having substantial public interest.

- TECHNICAL TRANSLATION. English-language translations of foreign scientific and technical material pertinent to NASA's mission.

For more information about the NASA STI program, see the following:

- Access the NASA STI program home page at http://www.sti.nasa.gov

- E-mail your question to help@sti.nasa.gov

- Fax your question to the NASA STI Information Desk at 757-864-6500

- Telephone the NASA STI Information Desk at 757-864-9658

- Write to:
  NASA STI Program
  Mail Stop 148
  NASA Langley Research Center
  Hampton, VA 23681-2199

NASA/TM—2020-220380

Durability of YSZ Coated Ti_2AlC in 1300 °C Mach 0.3 Burner Rig Tests

James L. Smialek
Glenn Research Center, Cleveland, Ohio

Michael D. Cuy
Vantage Partners, LLC, Brook Park, Ohio

Bryan J. Harder
Glenn Research Center, Cleveland, Ohio

Anita Garg
The University of Toledo, Toledo, Ohio

Richard B. Rogers
Glenn Research Center, Cleveland, Ohio

Prepared for the
Materials Science & Technology (MS&T)
sponsored by MS&T
Portland, Oregon, September 29–October 3, 2019

National Aeronautics and
Space Administration

Glenn Research Center
Cleveland, Ohio 44135

February 2020

Acknowledgments

The authors are grateful to Joy Buehler for metallographic preparation and Dan Scheiman for Raman spectra. This work was sponsored by the transformational technology task of the NASA Fundamental Aeronautics program.

This work was sponsored by the
Transformative Aeronautics Concepts Program.

Level of Review: This material has been technically reviewed by technical management.

Available from

NASA STI Program
Mail Stop 148
NASA Langley Research Center
Hampton, VA 23681-2199

National Technical Information Service
5285 Port Royal Road
Springfield, VA 22161
703-605-6000

This report is available in electronic form at http://www.sti.nasa.gov/ and http://ntrs.nasa.gov/

Durability of YSZ Coated Ti_2AlC in 1300 °C Mach 0.3 Burner Rig Tests

James L. Smialek*
National Aeronautics and Space Administration
Glenn Research Center
Cleveland, Ohio 44135

Michael D. Cuy
Vantage Partners, LLC
Brook Park, Ohio 44142

Bryan J. Harder
National Aeronautics and Space Administration
Glenn Research Center
Cleveland, Ohio 44135

Anita Garg
The University of Toledo
Toledo, Ohio 43606

Richard B. Rogers
National Aeronautics and Space Administration
Glenn Research Center
Cleveland, Ohio 44135

Abstract

A thermal barrier coating system survived burner rig testing at 1300 °C for 500 h. A 160 μm thick yttria stabilized zirconia (YSZ) coating was applied to a Ti_2AlC MAX phase bar sample by plasma spray physical vapor deposition (PS-PVD) and tested face-on in an atmospheric Mach 0.3 jet fuel burner, using 5-h thermal cycles. No thermal barrier coating (TBC) spallation or recession was observed, only a 2.4 mg/cm^2 mass gain. The modest weight gain precluded severe volatility losses under high velocity burner conditions. The coating surface exhibited colonies of $(111)_{flourite}$ fiber-textured columns separated by craze patterns, with no visible moisture attack. The metastable tetragonal t' YSZ phase was obtained initially, transitioning to equilibrium t_{eq} and cubic YSZ, but with little detrimental monoclinic. The thickness of the alumina TGO was ~21 to 23 μm under the heated YSZ face and ~13 to 15 μm on the uncoated, cooler backside. The backside exhibited removal of initial transient TiO_2 nodules and partial etching of the underlying Al_2O_3 scale by volatile hydroxides formed in high temperature, high velocity water vapor. Aerodynamic forces produced some bending of the cantilevered sample via creep. The test indicated exceptional stability of YSZ coatings on Ti_2AlC under turbine conditions, with thermal expansion matching playing a key role. The purpose of this study was to demonstrate long term durability of YSZ/MAX phase system in aggressive high temperature burner rig testing.

*Distinguished Research Associate, retired

Introduction

MAX phases have been keenly studied because of their unique crystal structure and intriguing properties (Refs. 1 and 2). Having $M_{n+1}(Al,Si)(C,N)_n$ general composition, they are defined as ceramics, but possess unusual desirable attributes such as high conductivity, thermal shock resistance, easy machinability, and deformation tolerance. The mechanical properties derive from weak M-(Al,Si) bonding in the basal plane that leads to sliding and kinking in preference to catastrophic crack growth. Like most ceramics they are phase stable at high temperatures, generally up to 1500 °C. High temperature oxidation resistance is excellent for alumina-forming Ti_3AlC_2, Ti_2AlC, and Cr_2AlC, as reviewed by Tallman, et al. (Ref. 3). Compatibility with α-Al_2O_3 scales is further enhanced in cyclic exposures by a close matching of thermal expansion coefficients, (Ref. 4) i.e., (~9.3, 10.2, 11.3×10^{-6}/K for Al_2O_3, Ti_2AlC, and YSZ, to be discussed).

Turbine environments generally contain 10 percent water vapor in the combustion gases, therefore moisture effects can be a concern for some materials (Ref. 5). Furnace tests of MAX phases in high temperature steam generally showed little effect on Al_2O_3 scale growth (Ref. 6). However, high velocity and high pressure gas can influence scale losses by the formation of volatile reaction products, such as $TiO(OH)_2$ and $Al(OH)_3$ (Refs. 7 to 10). This phenomenon had been discussed for 1100 to 1300 °C high pressure burner rig tests of Ti_2AlC (Ref. 11). A single cubic growth rate parameter k_{cubic} was measurably lower than comparable furnace TGA data, but it could be matched reasonably well if corrected for a slight volatility term. In general, a two-parameter cubic-linear growth-volatility law was believed to apply. Corresponding scale volatility loss rates, directly measured at 1300 °C on a pre-oxidized sample, were moderate (0.012 mg/cm^2/h) and largely attributed to removal of the initial TiO_2 transient scale.

A related CH_4 burner study of high purity Cr_2AlC MAX phase demonstrated 1200 °C durability after 500 rapid (5 min. heat and 2 min. cool) thermal shock cycling (29 h hot time) (Ref. 12). Heating and cooling rates were ~1000 and 500 °C per minute, with a gas velocity of 5 m/s, producing a 75 °C/mm gradient. A 7 μm Al_2O_3 surface scale and a 13 μm Cr_7C_3 depletion zone formed with no signs of failure. No evidence of scale volatility was evident, although weight change was not provided, the velocity was moderate, and the total hot time was not extensive. The same high gradient BRT was used to produce 1400 °C surface temperatures for a YSZ/Cr_2AlC/IN738 system in the first study of MAX phases used as bond coats for thermal barrier coatings (TBC) (Ref. 25). Here TBC failure was reported after 745 cycles, with only a 1.5 μm Al_2O_3 scale entrained within a porous, Cr_7C_3 bondcoat depletion phase.

YSZ thermal barrier coatings have been considered to be a compatible complement to Al-MAX phases because of thermal expansion matching and *extremely* low volatility in water vapor. Initial studies showed superior oxidative stability up to 1300 °C, for long times (at least 500 h) for Ti_2AlC substrates and less (268 h) for Cr_2AlC, while withstanding large alumina TGO scale thickness (~35 to 40 μm) (Refs. 13 and 14). By comparison, typical superalloy systems can only survive 1150 °C maximum interface temperatures for extended periods, with a maximum sustained TGO below 10 μm (Ref. 15).

High temperature SiC based systems are known to form slow-growing SiO_2 scales. But these are subject to rate enhancement and volatile $Si(OH)_4$ products in the presence of water vapor, as described comprehensively by Opila, et al. (Refs. 5, 16 to 19). Net weight losses are generally observed in high velocity, high pressure burner rig studies (e.g., 0.084 mg/cm^2/h at 1300 °C) (Ref. 20). Furthermore, the loss rates have been shown from chemical physics to scale with $v^{1/2}$ and $p_{H2O}{}^2$ (Ref. 16). Low activity, moisture-resistant environmental barrier coatings (EBC), such as rare earth silicates, are needed to prevent substrate recession under turbine conditions (Refs. 21 to 23).

YSZ is eminently qualified as a nonreactive moisture resistant material (Ref. 24), but with a coefficient of thermal expansion (CTE) too large to be compatible with SiC. For this and the points raised previously, it is, however, seen as a natural complement to MAX phases. Indeed, recent burner tests of YSZ TBC coated Cr_2AlC bond coats have shown potential above 1200 °C (Ref. 25). TBC/EBC protection of MAX phases in high velocity water vapor environments is therefore intriguing. The purpose of the present study was to demonstrate the durability of a 7YSZ TBC/Ti_2AlC system under aggressive 1300 °C Mach 0.3 burner conditions for 500 h. While this atmospheric burner set up is not high pressure, its simplicity does allow for long term, cyclic endurance testing. A secondary objective is to examine the oxidation/volatility behavior of uncoated Ti_2AlC regions exposed to the same environment.

Materials and Experimental Methods

Sample Preparation

The material tested in this study was Sandvik Kanthal (MAXthal 211) Ti_2AlC MAX phase obtained in the form of large sintered ingots. Two slabs 6.4×38×82 mm (1/8×1½×3¼ in.) were EDM machined from the ingot and hand polished thru coarse (60, 30, 15 μm) diamond wheels and finished with finer SiC carborundum grits to a 2400 grit finish. A duplicate sample was prepared to this finish on both sides and lightly grit blasted for coating adhesion.

Thermal Barrier coating was accomplished in a Sulzer-Oerlikon-Metco plasma spray physical vapor deposition (PS-PVD) facility at the NASA Glenn Research Center. Samples were coated normal to the torch with a standoff of 1.68 m. The torch power was 94 kW, plasma gases were 40/80 Ar/He, and the feedstock powder was Metco 6700 7YSZ. Coatings were deposited in 1.51 mbar (1.13 torr) partial vacuum, mostly via the vapor phase, achieving approximately 160 μm of YSZ in a segmented columnar 'cauliflower' microstructure, similar to traditional EB-PVD structures. Both samples were given a mild preconditioning furnace oxidation exposure at 1000 °C for 10 h. This helped insure against any unexpected, premature 'infant mortality' failure and to insure the YSZ coated sample was first transformed to 'white' ZrO_2 from the 'black' oxygen-deficient PS-PVD as-deposited structure. Bulk alumina coupons were also coated for YSZ deposition studies and given various thermal treatments as needed for characterizations described later.

About 1/2 in. (11 mm) strip was cut across the width from one end of each sample after the 10 h initialization treatment of the full slabs. These were used as bare and coated witness samples in interrupted furnace oxidation tests at 1000 to 1300 °C, in successive 50° increments. The intent here was to have baseline oxidation data from pieces of the same samples used in similar stepped Mach 0.3 burner rig tests at the same temperatures, i.e., remnant plates (slabs) used in the burner rig.

Burner Test Protocol

The bare slab sample was tested first as a preliminary shake out run and baseline comparison for the coated sample. In addition to overall oxidative durability, information regarding moisture induced scale volatility was obtained, given that the combustion gas contained about 10 percent water vapor and was flowing at about 100 m/s (as compared to 25 m/s in the previous high pressure burner rig (HPBR) tests). Automatic cycling to ambient temperature was produced every 5 h, with weighing and inspection over graduated time intervals.

A description of the atmospheric Mach 0.3 burner can be found in Reference 26. The rig utilized 120 psig (800 kPa) filtered shop air measured with turbine flow meters (data logged) and rotometers (visual). At Mach 0.3, approximately 1.1 kg (2.5 lb)/min airflow was used (with up to 3.2 kg (7.0 lb)/min possible for higher Mach numbers). Preheated 288 °C (550 °F) air was mixed with atomized Jet-A fuel in a swirl plate nozzle and delivered to the combustion chamber. Pressure within the combustor was 1 psi (6.9 kPa) above ambient to produce Mach 0.3 flame velocity. An aircraft-type igniter initiated combustion. The inner liner was made of Inconel 601 with about a 2 in. (5.08 cm) inner diameter and a 1 in. (2.54 cm) exit nozzle. Flame temperature was monitored by thermocouple and sample temperature by optical pyrometer (8 μm wavelength for YSZ, emissivity set at 0.92, and 2-color pyrometer for bare Ti_2AlC MAX phase). Temperature was controlled ±5 °C by a feedback loop between the optical pyrometer (sample temperature) and the fuel flow control valve that adjusted the fuel-to-air ratio. Cycling every 5 h was produced by pneumatically pivoting the burner apparatus away from sample impingement. No backside cooling was used in these tests. Sample weights were measured on an analytical balance sensitive to 0.01 mg.

The burner facility is shown in Figure 1. The schematic illustrates the key components of the burner, Figure 1(a), while the photograph illustrates the actual burner in operation, Figure 1(b). Here, initially, the full slab was used for the test, clamped with a vise. (Later, sample strips were sectioned lengthwise and mounted via set screw in a slotted superalloy mounting pedestal). The same stepped thermal sequence as the furnace witness sample was attempted for the uncoated sample, *face-on*, perpendicular to the flame, Figure 2, resulting in a very uniform temperature distribution over the sample midsection. Furthermore, because of the excellent thermal conductivity of this MAX phase ($k_t \approx 30$ W/m·K), the backside temperature was only about 10 °C lower (Ref. 2). This orientation deflected the entire flame and resulted in overheating of the test cell, even after attempts to modify the exhaust ducting. After 50 h at 1000 °C and 50 h at 1100 °C, the screening test was changed from *face-on* to *edge-on* heating in order to reach 1200 and 1300 °C.

The next sequence involved the TBC coated slab, keeping the edge-on configuration to allow maximum temperatures to be achieved. However, edge-on exposure of the YSZ coated slab resulted in a crack upon initial heating, necessitating test termination and a new approach.

1200 °C Shakedown Test

Two 13 mm wide coated specimens were salvaged from this slab by sectioning along the length of the YSZ coated slab. One was fastened to a slotted sample pedestal and secured with steel shims and a set screw at one end (see schematic in Figure 1(a)). It was positioned face-on in the burner and subjected to a shakedown exposure achieving 1200 °C surface temperature, using 5-h cycles. Here some coating abrasion was observed in the grip end, from clamping with the shims and set screw. The coating was removed here by light grinding with a hand held Dremel-type diamond tool after the first 100 h of testing. The test was terminated after 500 h with no further anomaly.

The preliminary testing above thus identified the following shortcomings and resolution: 1) insufficient thermal flux for face-on, uncoated, full slab test; 2) edge cracking/breakaway oxidation after 1300 °C edge-on testing of the uncoated slab; 3) edge crack during initial heating of edge-on YSZ coated slab; 4) grip end coating abrasion for face-on heating of coated strip sample; 5) successful 1200 °C test completion (500 h) of that sample after grip end coating removed (100 h).

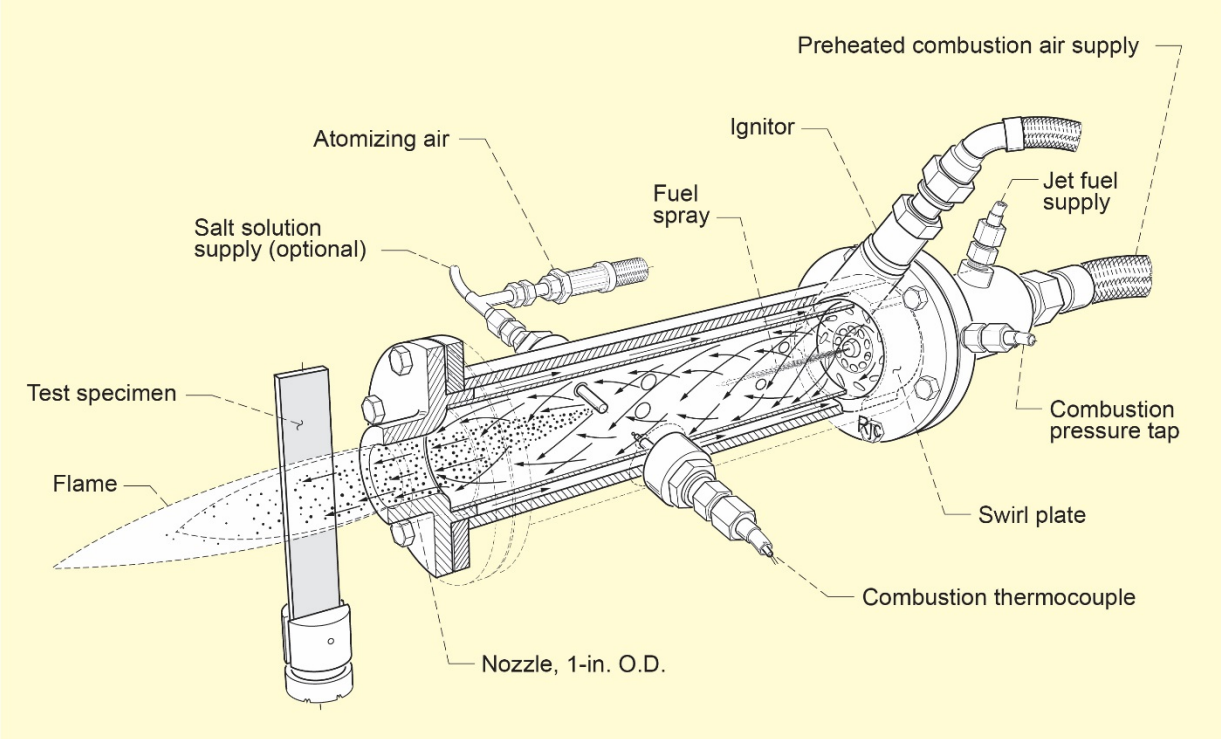

(a)

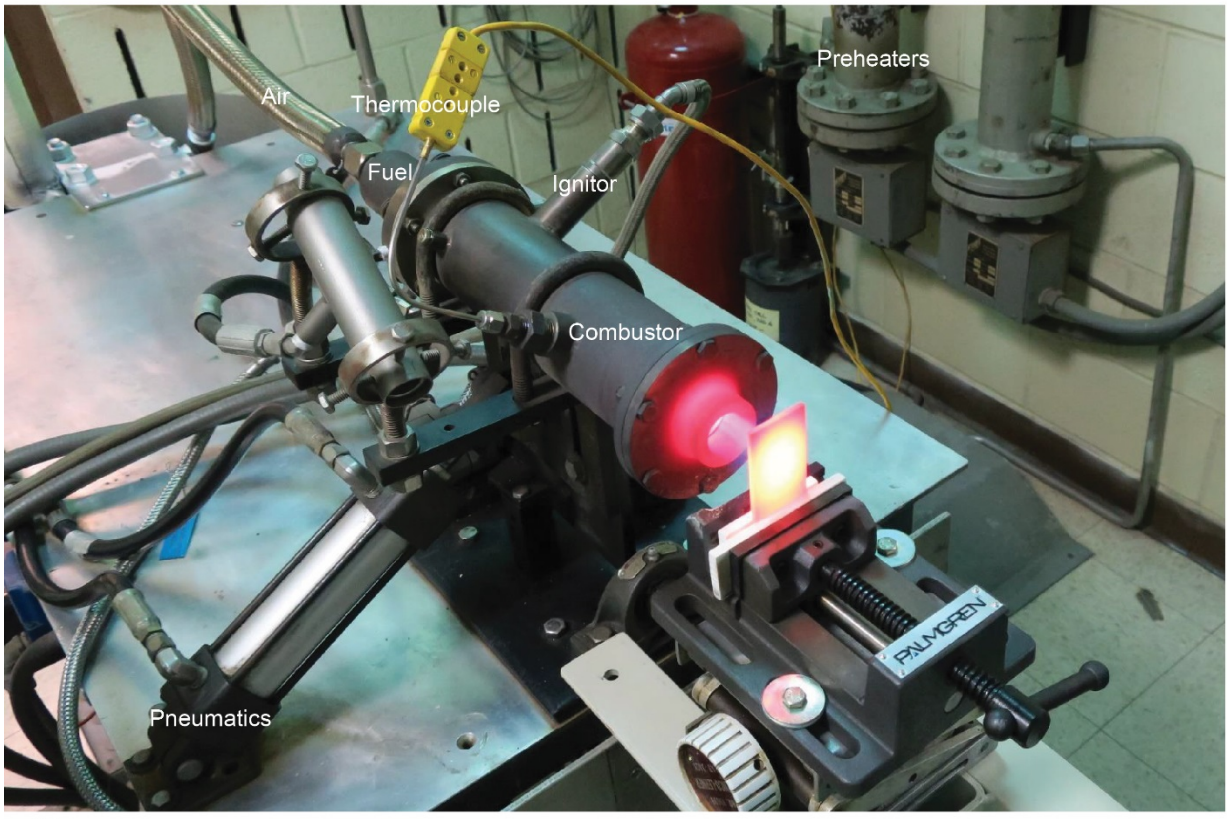

(b)

Figure 1.—Mach 0.3 burner rig. (a) Schematic of operational features. (b) Photo of running burner. Uncoated slab sample, vise mounted.

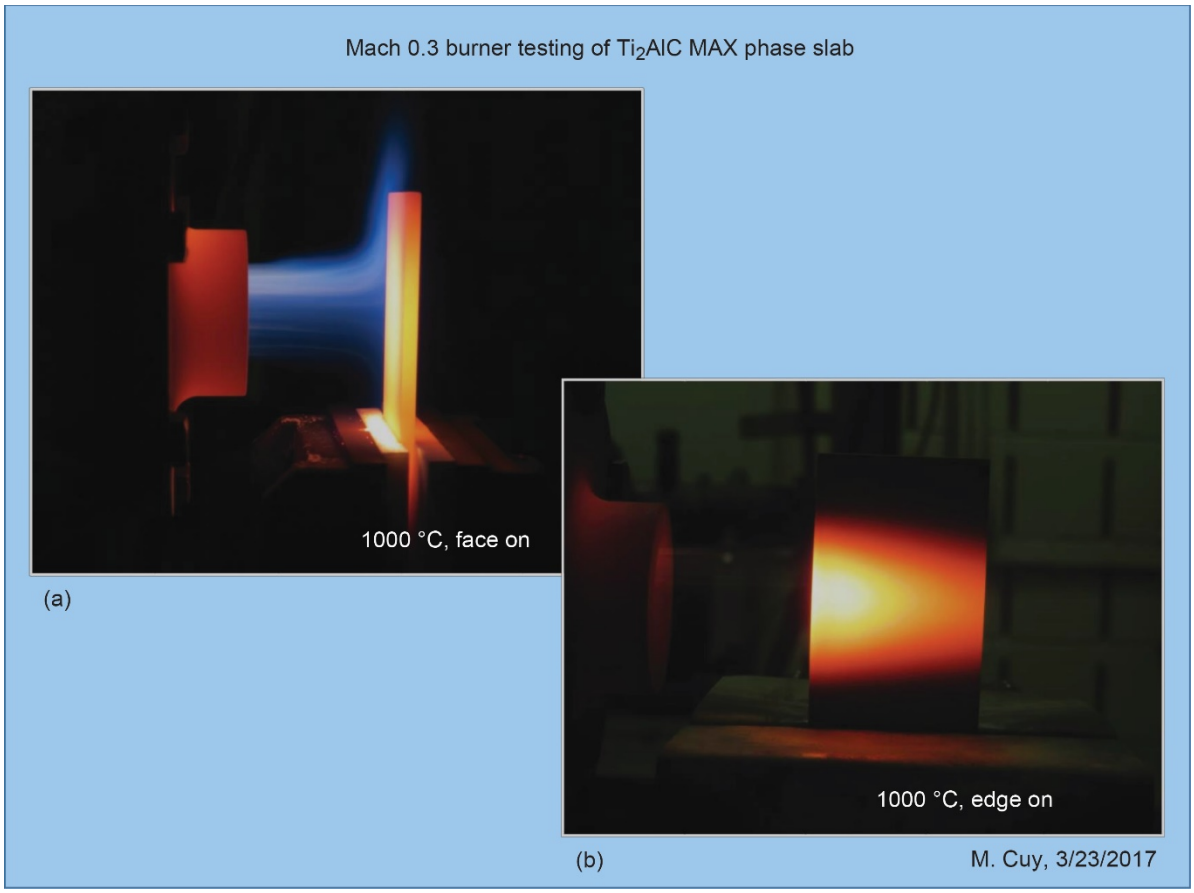

Figure 2.—Photographs of burner flame impingement on uncoated Ti_2AlC slab sample. (a) Face-on orientation. (b) Edge-on orientation.

Target 1300 °C Durability Test

The test protocol arrived at above was used for the second YSZ-coated strip. Sample dimensions were 3.6×15.2×62.3 mm. The coating was first ground off in the grip end region, leaving about 50 mm exposed to the 25 mm diameter combustion flame. The front surface coating temperature was set to 1300±5 °C, controlled by the 8 μm pyrometer (e = 0.92) and fuel-air ratio. Further measurements were obtained by 2-color optical pyrometer for the bare backside and thermocouple in the combustion gas. Deflection was also monitored by caliper measurements of the bending gap between the ends and curved center.

Analyses

Microstructures were characterized by optical microscopy and SEM of surfaces and Ni-plated polished cross sections at 15 kV (Hitachi S-4700 FESEM, Tokyo). X-ray diffraction analyses (XRD) were used to identify coating and oxide phases, (Malvern Panalytical Empyrean diffractometer, Westborough, Massachusetts) using Co Kα radiation and (Bruker, D8 Advance diffractometer with Cu Kα radiation, Madison, Wisconsin) from both sides of the sample. The instrument was configured to limit the beam width to 5 mm and prevent spillage off the face of the sample at all diffraction angles. A 5-axis cradle was used to achieve desired sample orientations. The ICDD 2018 PDF4+ Inorganic database and Jade 2010 software. Raman spectra were obtained on select YSZ coatings as a more sensitive technique for identifying YSZ phases (Thermo Scientific, originally Nicolet, DXR microscope, Waltham, Massachusetts). Operating conditions were 1 sec, 633 nm laser at 5 mW, 600 lines/mm, 25 μm pinhole.

Results

Witness Furnace Tests and Preliminary Burner Exposures

The furnace data for the bare witness sample was completely normal, as shown in Figure 3. There was an initial abrupt uptake in the first hour corresponding to the typical rapid growing transient TiO_2 scale. Eventually this tapered off to the slow kinetics representing protective Al_2O_3 scales. This continued for the initial 50 h at 1000 °C and proceeded through subsequent exposures at 1100, 1200, and 1300 °C as well. The test was stopped after 50 h at 1300 °C, achieving a 3.60 mg/cm^2 total weight gain.

Pre-exposure of the YSZ coated witness sample commenced during the 1 torr low pO_2 oxidation that occurs in the PS-PVD vacuum chamber during coating. This effectively limits the amount of initial TiO_2 transient and reduces subsequent weight gains. The weight change shown in Figure 3 is consistent with protective Al_2O_3 scales. They are lower than those of the uncoated sample by ~0.2 mg/cm^2 after 10 min. at 1000 °C, then by 0.66 mg/cm^2 at the end of the test. No spalling or degradation of the YSZ coating was exhibited in this furnace demonstration.

The weight change behavior of the uncoated burner slab is presented in Figure 4. The 1000 °C *face-on* test (F) showed losses initially, slowing with time. This is interpreted as volatility effects, presumably accentuated by the large amount of transient TiO_2 formed early then removed by the high velocity burner gas stream. The associated flow patterns are shown in Figure 5. After 50 h, the temperature was increased to 1100 °C, where a slow rise in weight gain was realized.

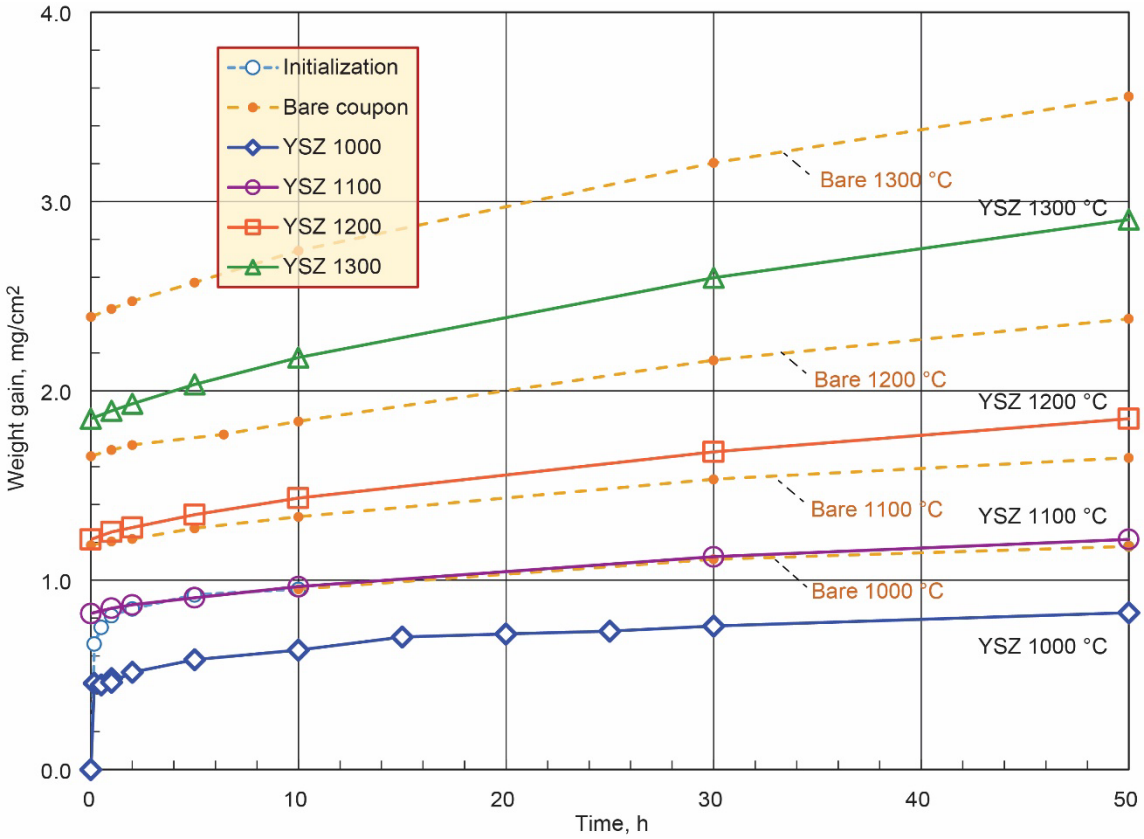

Figure 3.—Stepped furnace oxidation of YSZ Coated Ti_2AlC (solid curves) compared to uncoated Ti_2AlC (dashed curves). Coated sample exhibits lower average weight gain. (1000 to 1300 °C, 50 h at each temperature).

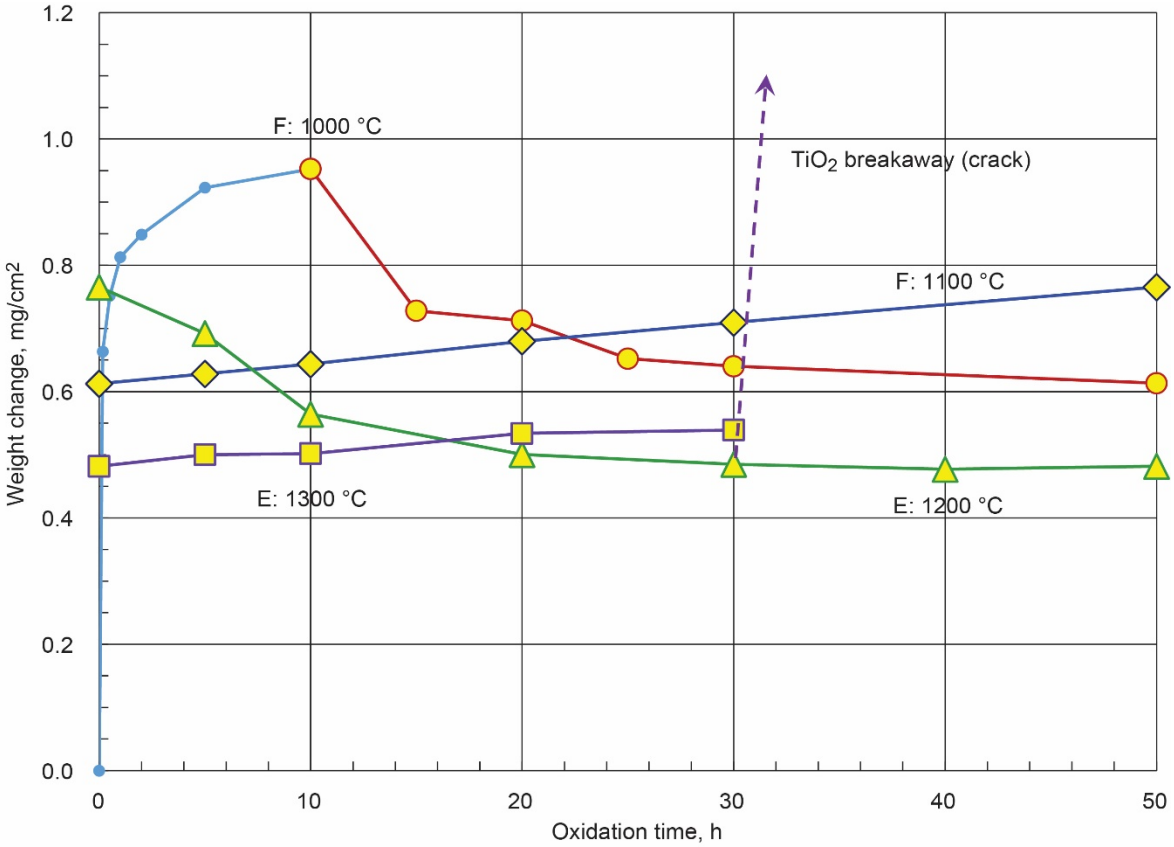

Figure 4.—Weight change behavior of 1000 to 1300 °C stepped burner test of uncoated Ti_2AlC slab sample. (10 h furnace preconditioning at 1000 °C). Initial (F) Face-on and (E) edge-on exposures resulted in a gradual loss, then gain, when stepped to higher temperatures.

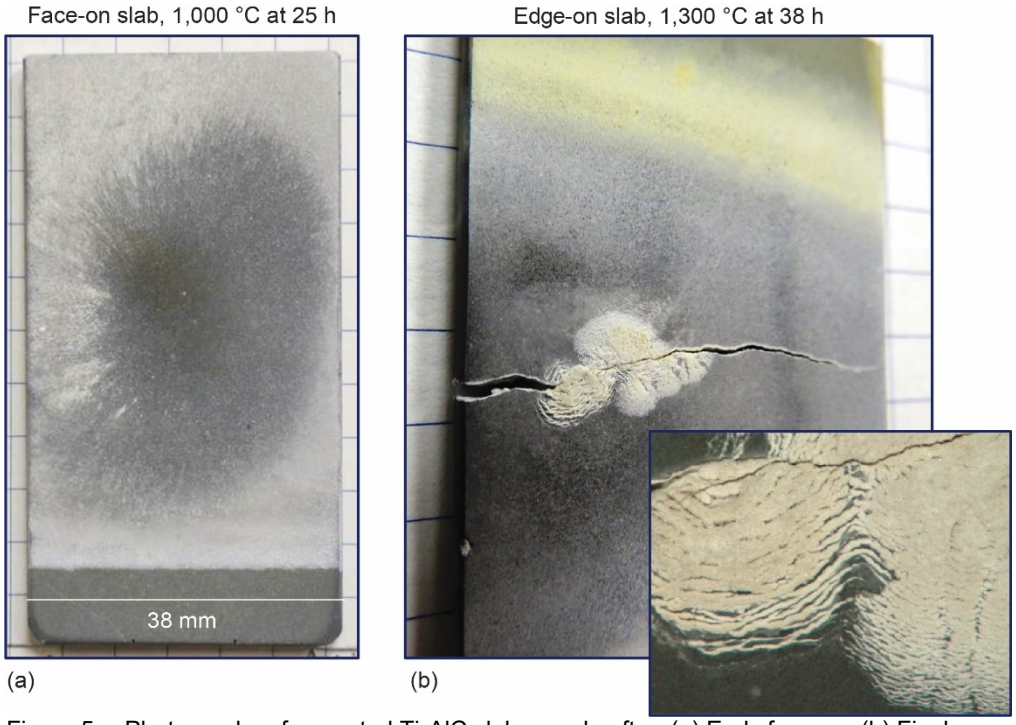

Figure 5.—Photographs of uncoated Ti_2AlC slab sample after. (a) Early face-on. (b) Final edge-on burner exposures: cracking and breakaway TiO_2 growth after 38 h at 1300 °C.

Edge-on exposure at 1200 °C (E) again produced losses. This was presumably due to residual TiO_2 removed from the backside, now exposed more directly to high velocity gas impingement and exhibiting fading white flow lines on that side of the sample. Then gains occurred at 1300 °C, until, after 30 to 38 h, an anomalous runaway oxidation event took place with catastrophic TiO_2 growth and a gain of 4.4 mg/cm^2. This was perhaps triggered by a leading-edge crack, Figure 5. The multiply-striated TiO_2 advancing oxidation front is typical of anomalous Ti_2AlC damage-induced attack, perhaps due to alternate layers of rapid attack, then Ti depletion and Al_2O_3 reformation (Ref. 27). The slab cracked almost entirely across the midspan and the test was terminated.

Edge-on exposure of the YSZ coated slab resulted in a crack upon initial heating, Figure 6, necessitating test termination. Here a leading-edge crack was observed on initial heat-up, after only 10 min, up to 927 °C (1700 °F). The crack, while very narrow, did extend through the thickness of the sample and extended ~1/3 across the width. Again, some anomalous thermal shock or material defect was suspected, and the test was terminated. No definitive explanation of crack origins was obtained for either slab test.

Consequently, face-on testing of narrow strips cut from the coated slab was adopted, starting at 1200 °C. The overall appearance throughout 1200 °C testing is presented in Figure 7. Little effect was observed on the TBC. The raw weight change results are presented as the dashed curve in Figure 8. The initial coating abrasion loss (up to 100 h) was eliminated by coating removal in the grip region. A gradual oxidation gain was then observed for the remainder of the test (500 h). An approximate corrected curve (solid line) was constructed by re-zeroing all the losses up to 100 h. The final gain after 500 h was only 1.0 mg/cm^2, achieving an average linear rate of only ~ +0.001 mg/cm^2/h. No cracks, breakaway oxidation, coating damage or spallation was observed. This success warranted the follow-on burner test at 1300 °C, the maximum temperature evaluated in successful 2500 h stepped furnace oxidation studies (Ref. 13).

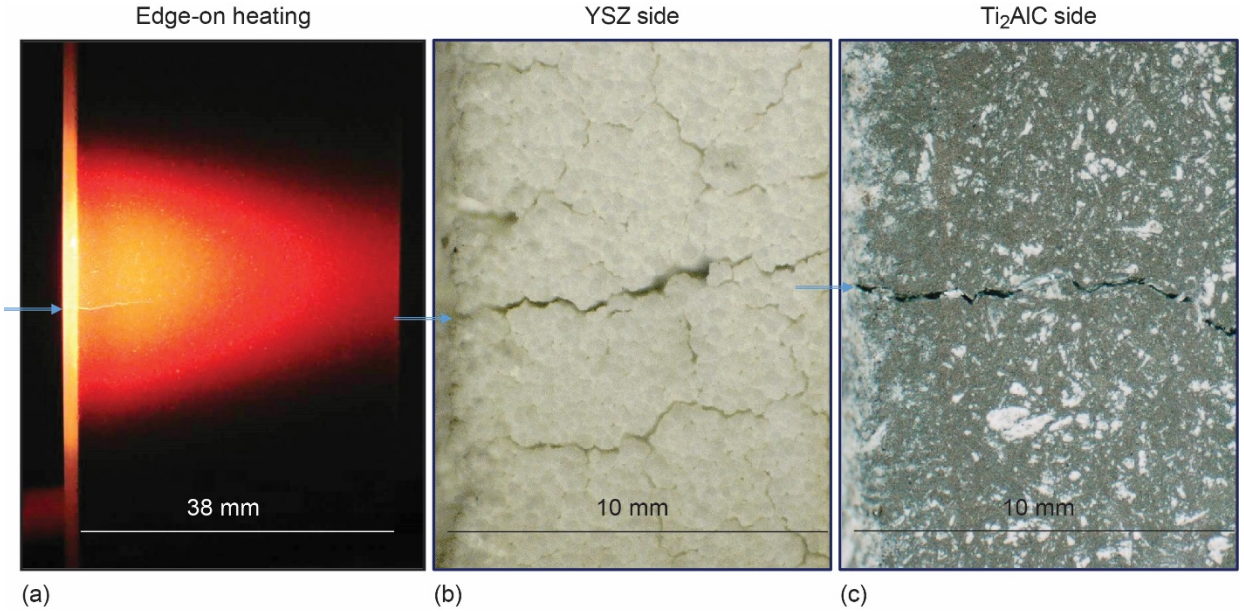

Figure 6.—Cracking on initial, edge-on, burner heat-up of YSZ-coated Ti_2AlC slab sample. (a) During test. (b) Coated side. (c) Uncoated side after cooldown.

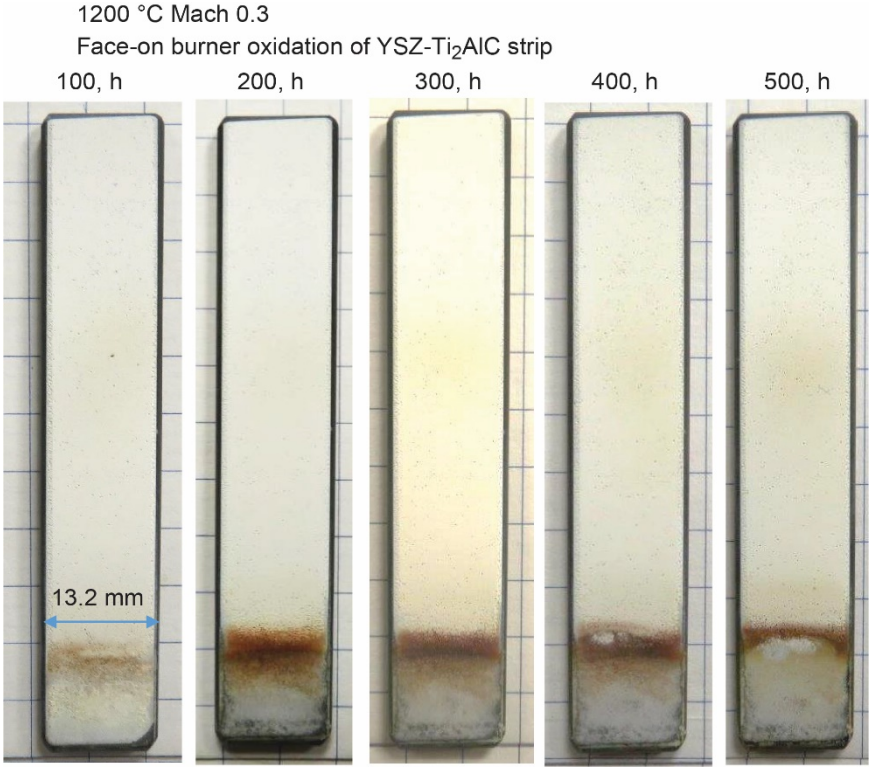

Figure 7.—Photographs of YSZ coated Ti_2AlC strip sample throughout 500 h, face-on, Mach 0.3 burner rig shakedown test at 1200 °C. No coating spallation. Abrasion at grip region was eliminated by grinding after 100 h of test.

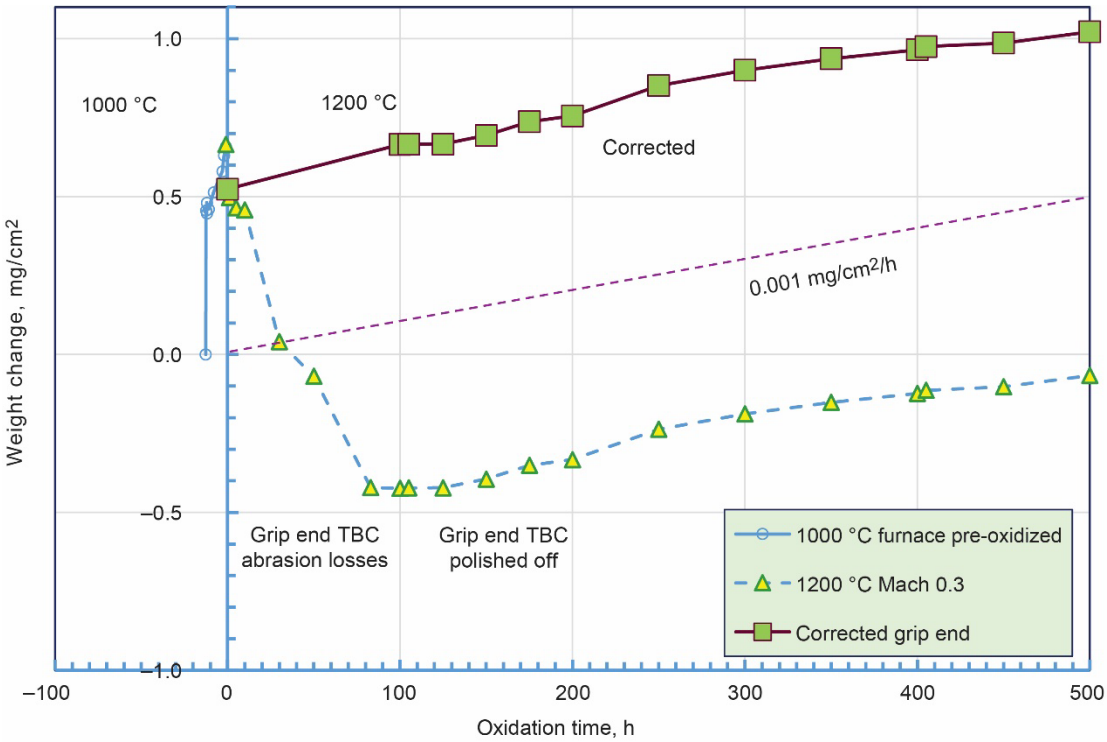

Figure 8.—Weight change behavior corresponding to YSZ-coated, Ti_2AlC strip sample in previous figure. Initial weight loss from gripping abrasion (triangles). Corrected for abrasion losses (squares). (Initial 10 h furnace conditioning, small circles).

1300 °C Mach 0.3 Burner Tests

The photographs in Figure 9 show the coated strip sample in the burner rig test (BRT). Photo (a) indicates the hot gas flow from the burner across the sample from a top right view angle. The mounting base, with FeCrAl and CMC shims, are visible below the hot zone of the sample. The sample hot zone corresponds to the 2.5 cm (1 in.) inner diameter of the exhaust nozzle, as observed in the low exposure photograph, (b). Photo (c) is a side view illustrating the bending that occurred after 425 h of testing. Finally, photo (d) is a top view showing the flare out and splitting of the luminous exhaust flame.

The weight change behavior of the YSZ-coated Ti_2AlC MAX phase sample is shown in Figure 10(a). The furnace pre-oxidation treatment at 1000 °C is presented as time before zero. It reflects a rapid growth of $TiO_2 + Al_2O_3$ scales to ~0.76 mg/cm^2 upon initial furnace pre-conditioning. The subsequent response to the BRT (burner rig test) is represented by the remainder of the curve. It shows a well-behaved, continuous behavior with decreasing oxidation rate, as occurs for common parabolic or cubic growth laws, and not suggestive of any spallation events. The final weight gain is a modest 2.40 mg/cm^2.

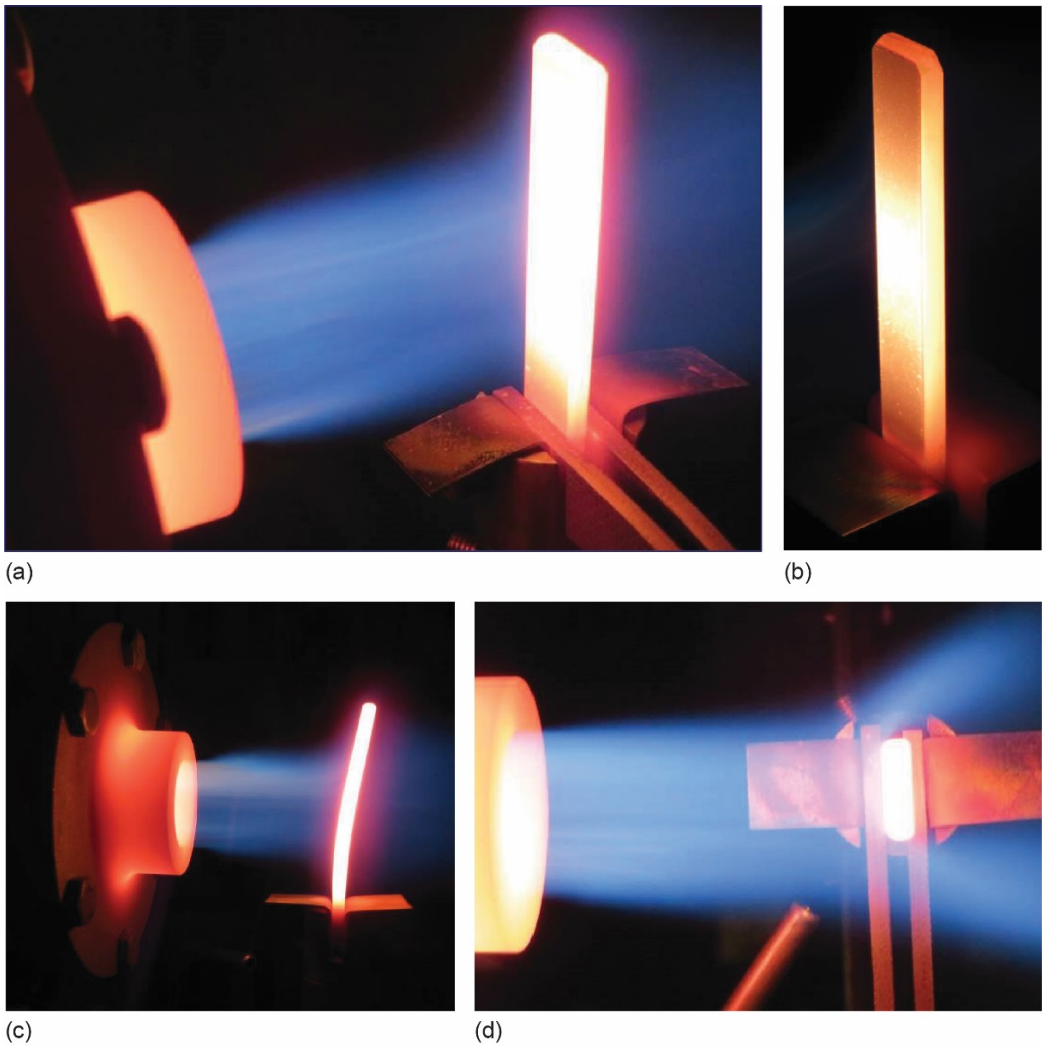

Figure 9.—Photographs of burner rig and YSZ coated Ti_2AlC MAX phase sample in operation. (a) Upper angled view showing flame, sample and mounting base. (b) Short exposure indicating temperature gradients along sample length. (c) Edge-on view showing bending due to aerodynamic force after 425 h. (d) Top view of flow lines showing splitting of flame due to face-on impingement.

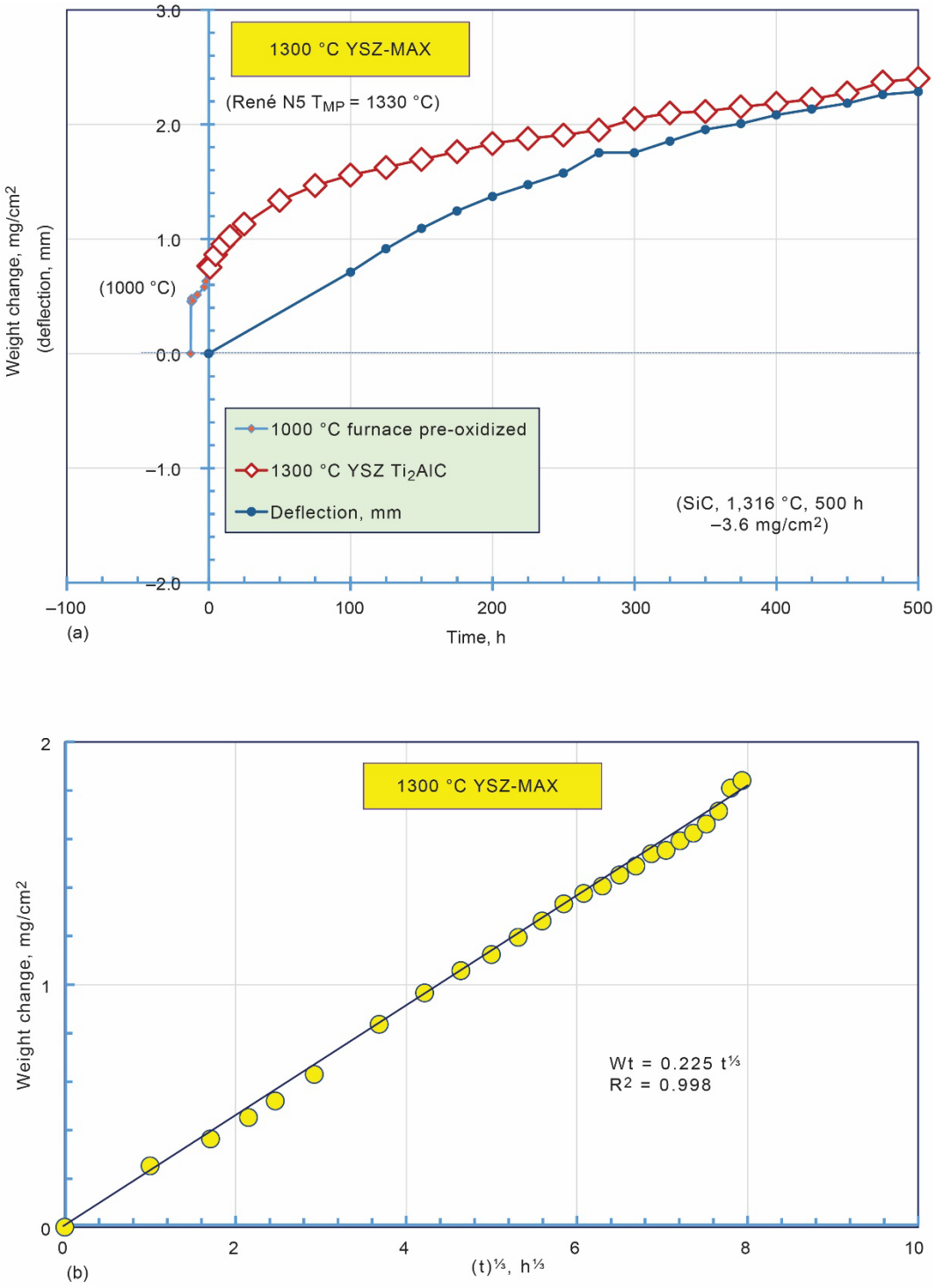

Figure 10.—BRT results: (a) Specific weight gain and degree of bending for 500 h Mach 0.3 1300 °C BRT. Deflection rate is slightly moderated with time as sample subtended area decreases. (b) Cubic oxidation kinetics (without spalling) is suggested by plotting transient corrected weight vs $t^{1/3}$.

This is less than the 4.55 mg/cm^2 calculated from the cubic growth rate constant (5.229×10^{-11} kg^3/m^{6}s or 0.200 mg^3/cm^{6}h) measured for the same material by a furnace TGA kinetics. This isothermal test also produced an initial TiO_2 transient scale of 0.4 mg/cm^2, making the final predicted weight ~5 mg/cm^2, i.e., substantially higher than the 2.4 mg/cm^2 produced in the burner rig here. It was found that, by correcting the burner rig data for the initial transient TiO_2 formation by 0.5 mg/cm^2, a very good fit to cubic $t^{1/3}$ kinetics was again produced, Figure 10(b), with k_c = 0.012 mg^3/cm^{6}h (r^2 = 0.998, intercept = –0.008 mg/cm^2). More detailed comparisons will be presented and discussed later.

A comparison of the YSZ-Ti_2AlC Mach 0.3 HP-BRT results with uncoated SiC is presented in Figure 11. Overall, weight gains exhibited for Ti_2AlC are in contrast to weight losses due to SiO_2 scale volatility and recession (Ref. 20). Similar high pressure burner rig results are also presented with similar conclusions. The specifics and implications will be discussed in detail later.

The photos in Figure 12 present the appearance of the burner sample: YSZ coated front face before and after the test and the uncoated backside after test. (The coating was ground off at the grip end (dashed line) to avoid fretting in the clamp and anomalous weight losses). Brown discoloration above the grip resulted from Fe-oxide staining from the FeCrAl gripping shims. The backside was relatively uniform, with slight lightening due to oxidation.

The photo in Figure 13 shows the total bending after the 500 h test, as monitored by the chord width (Δ) of the curved sample. The continuous development of the curvature was presented in Figure 10. The measurements were started only after 100 h when they were first noticed. The deflection rate was somewhat less than linear because sample bending shortens the moment arm of maximum force. Work hardening may also decrease the rate of bending/deflection.

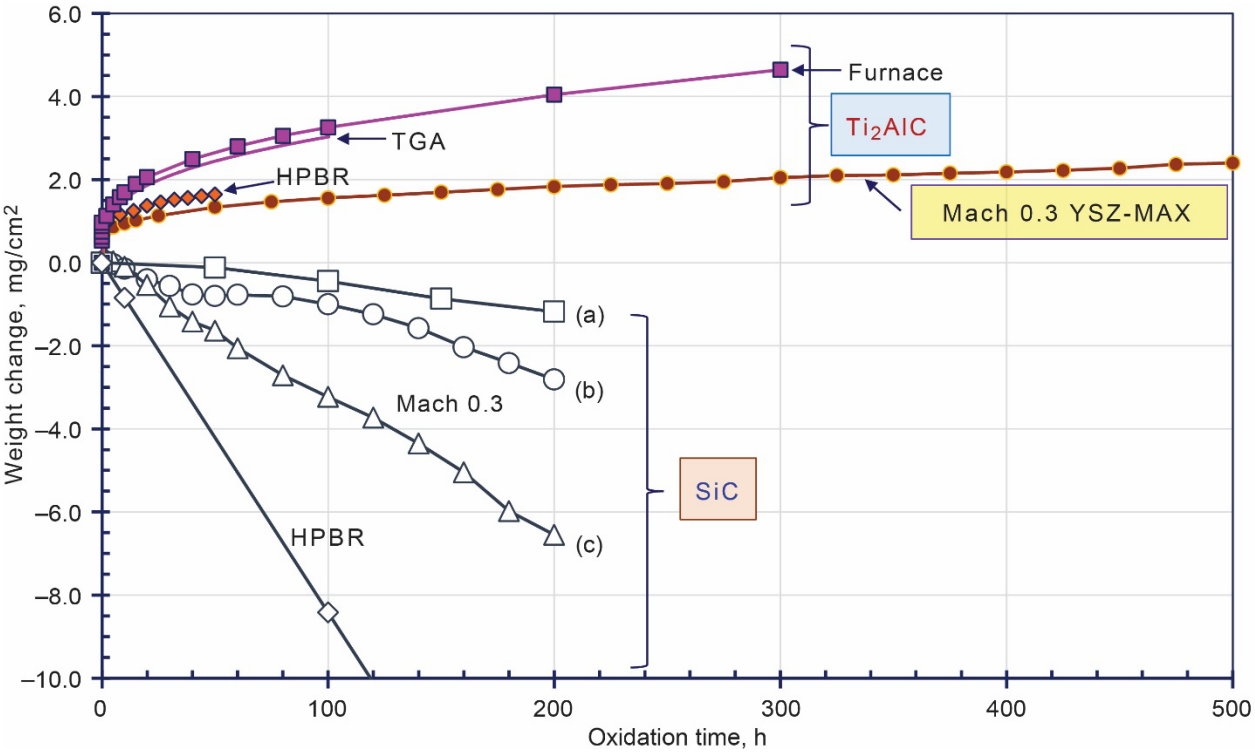

Figure 11.—Comparison of YSZ-MAX sample BRT oxidation data with other 1300 °C exposures in similar tests. (HPBR at 6 atm. and 20 to 25 m/s, TGA dry air, and ambient air furnace tests (Refs. 11, 13, and 37). Sintered 'Hexoloy' SiC curve (a) Reference 20, 1316 °C, (a,b) pyrometer sighted on edge; (c) sighted on face).

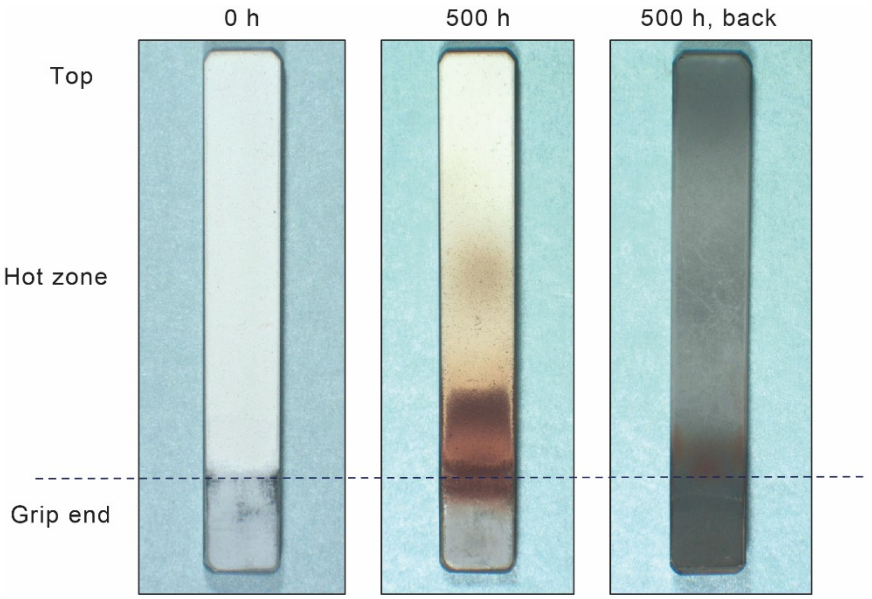

Figure 12.—Visual appearance of the YSZ-MAX strip sample before and after test. YSZ coating shows rust discoloration due to Fe transfer from Kanthal A1 FeCrAl mounting sheet. Coating ground off in mounting area to avoid abrasion losses.

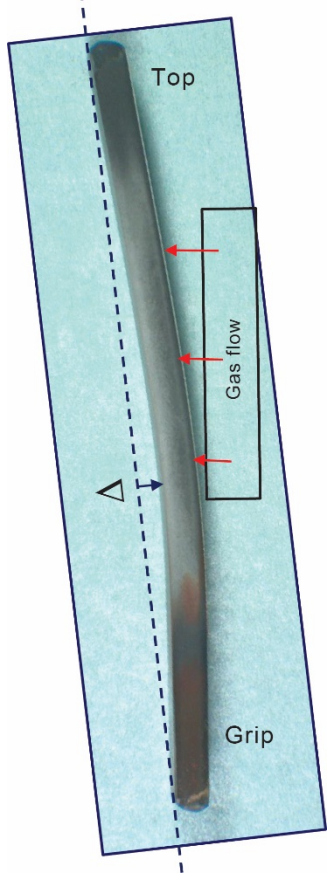

Figure 13.—Deflection due to creep from face-on, Mach 0.3 BRT flame impingement. (2.3.mm delta over 6.8 cm sample length. Lower ~1.5 cm gripped).

Microstructures

Coated Face

The optical micrographs in Figure 14 exhibit the overall surface structure of the coating after testing. The maximum temperature hot zone Figure 14(a) shows nodular colonies of columns, separated by wide-gap ‘cell’ mudflat craze crack boundaries. In contrast, the ‘warm’ zone surface, corresponding to the top of the bar, appears much more uniform. It may be that the hottest region fostered sintering and shrinkage, whereas the warm regions allowed expansion and compaction with respect to the cooler substrate. Sintering is a known phenomenon for YSZ thermal barrier coatings, especially above temperatures in the vicinity of 1250 °C.

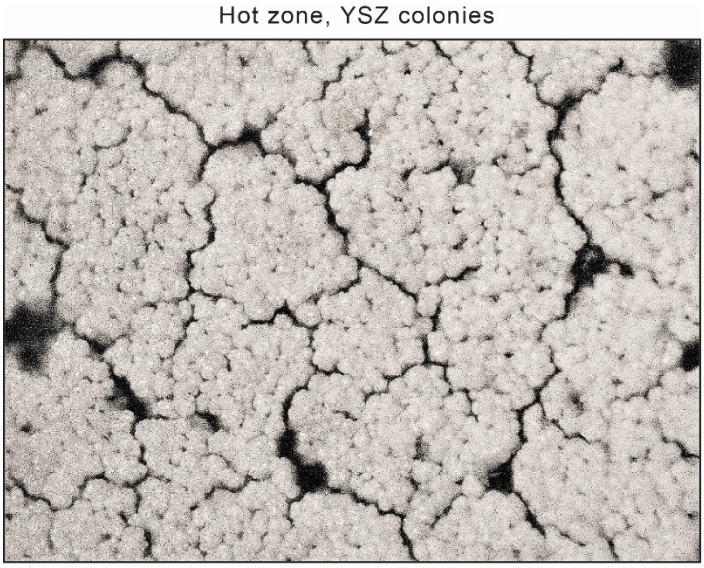

(a)

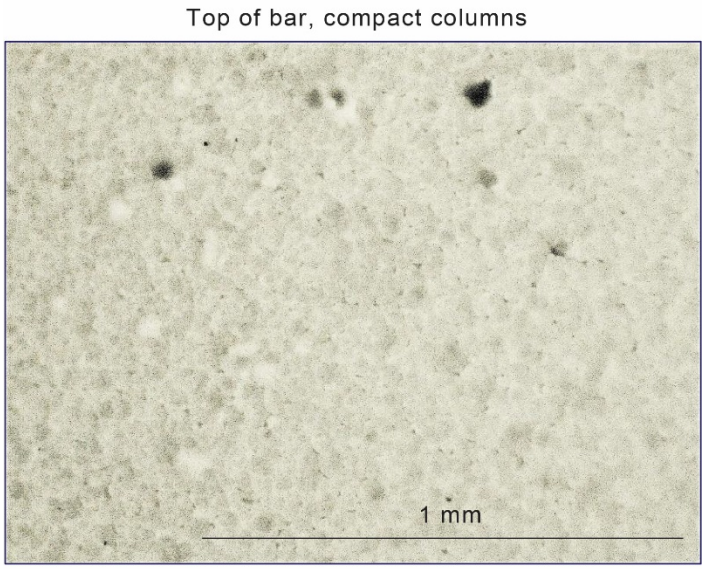

(b)

Figure 14.—Optical micrographs of coating surface after 500 h BRT at 1300 °C. (a) Shrinkage crazing pattern in hot zone. (b) Tight structure in cooler top end of sample.

SEM images of the coating growth columns in the hot section are given in Figure 15. At higher magnifications (Figure 15(b) and (c)), the granular surface structure of an individual column can be discerned, with ~1 to 3 μm grain diameters (2.6±0.6 μm, on average). No elemental peaks were observed in EDS spectra other than Zr, Y, and O.

Optical micrographs of polished cross sections of the tested coating are shown in Figure 16. The hot zone structures Figure 16(a) indicate an uneven YSZ surface, as encapsulated by Ni plating. The bulk of the ~160 μm thick coating exhibits a bimodal porosity—both finely dispersed and coarse columnar. Broad vertical separations, extending part way to the substrate, are frequently observed, corresponding to the craze patterns observed in plan views, Figure 14, Figure 15, with an average spacing of ~80 μm. However, no interface or through-cracks are observed in these or any other regions examined. By comparison, the YSZ structure near the cooler grip end Figure 16(b) shows most porosity highly aligned along prior YSZ columns boundaries. In general, these observations mirror those described in a recent study of 7YSZ PS-PVD coatings (Ref. 28).

At the MAX phase interface, the substrate is covered by an alumina scale, measured at the hot zone as 22.8 μm thick. At the cooler grip end, the alumina scale is 11.4 μm thick, or ~1/2 that in the hot zone, in accord with the lower temperature here. Different regions of the cross section may show slight differences in the measured thickness.

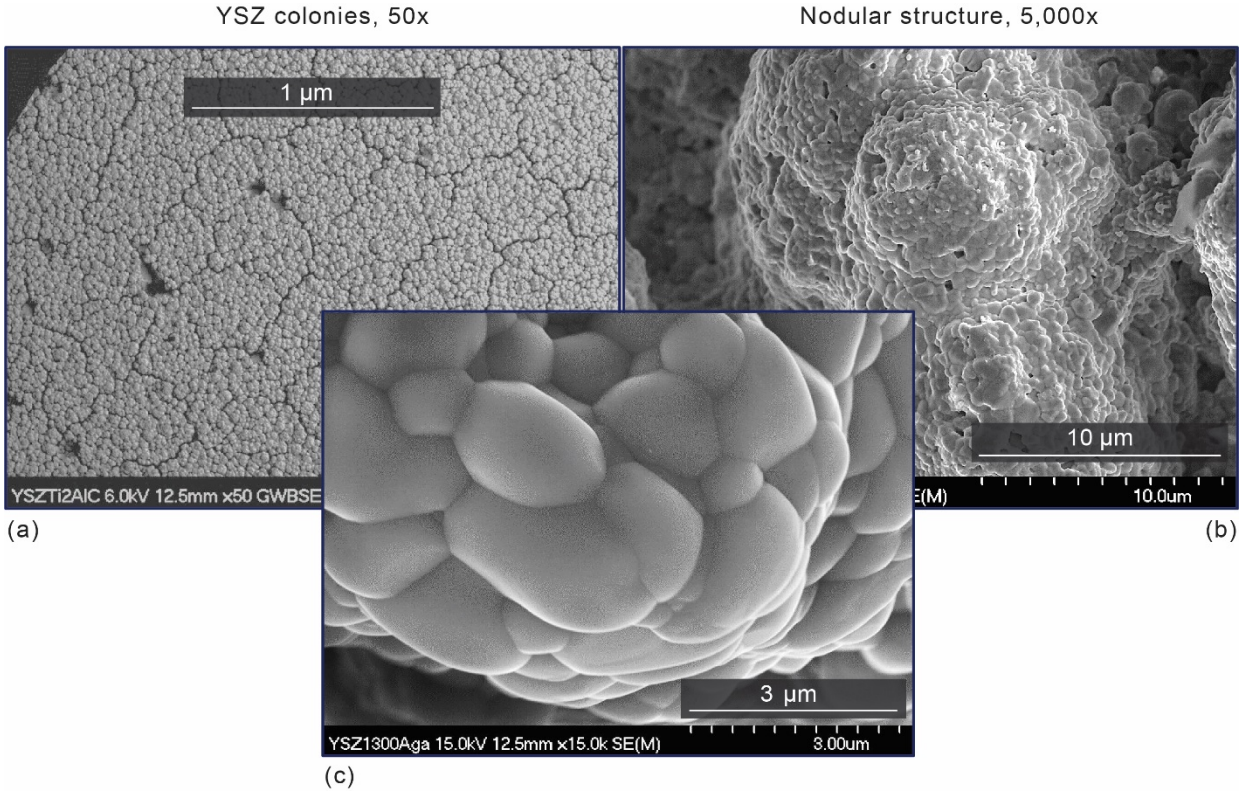

Figure 15.—SEM of YSZ coating surface after burner test. (a) Craze pattern shown in Figure 14. (b) Columnar PS-PVD deposition. (c) Pristine individual 1 to 3 μm YSZ grains on column surface.

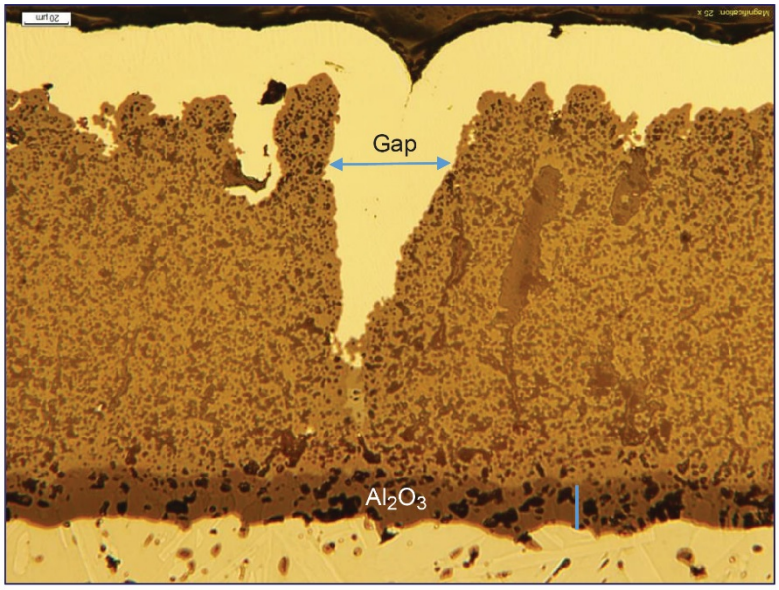

(a) Hot zone
22.8 μm TGO

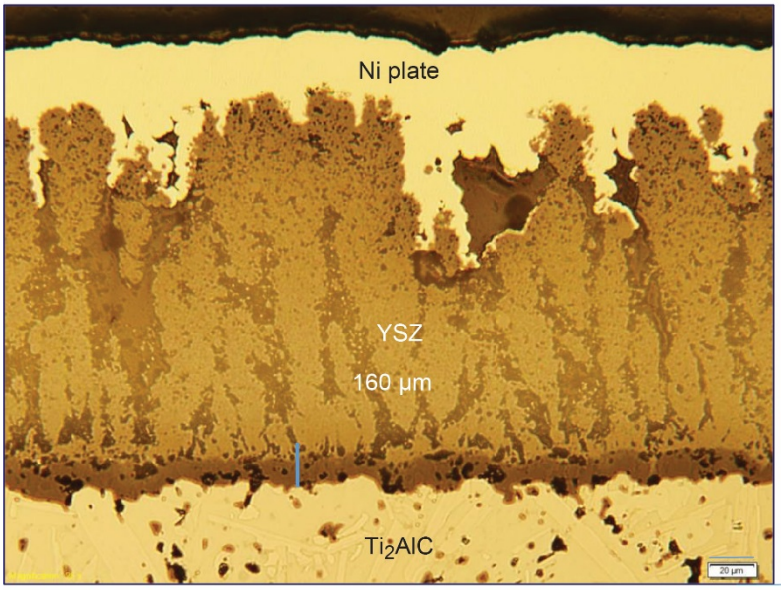

(b) Grip end
11.4 μm TGO

Figure 16.—Coated face optical micrographs; polished cross sections after 500 h BRT at 1300 °C (Ni-plated). (a) Hot zone ~160 μm thick YSZ, 22.8 μm thick alumina scale. (b) Cooler grip end aligned porosity, 11.4 μm thick alumina scale (20 μm scale bar).

The SEM images in Figure 17 reveal more details of the microporosity within the YSZ. Coarsening and uniform dispersal in the hot zone is compared to the regular arrays of fine as-coated porosity remaining at the grip end. Microporosity had been seen to coarsen in the recent PS-PVD study as well (Ref. 28). There is some porosity in the Al_2O_3 scale, but undoubtedly much metallographic pullout as well. The dark grey features in the Ti_2AlC MAX phase substrate were again identified as Al_2O_3 particles by EDS. No other first-order chemical inhomogeneity within the substrate, the Al_2O_3 TGO, or YSZ TBC was identified by EDS, although contrast variations can be seen at the YSZ/TGO interface. The alumina scale thickness was measured by SEM as 20.7 and 22.2 μm for two regions in the hot zone and as 12.4 μm in the grip end. These values are within experimental variations of those measured by optical microscopy above. The inner growth interface was again seen to follow a facetted morphology, following lenticular Ti_2AlC substrate features.

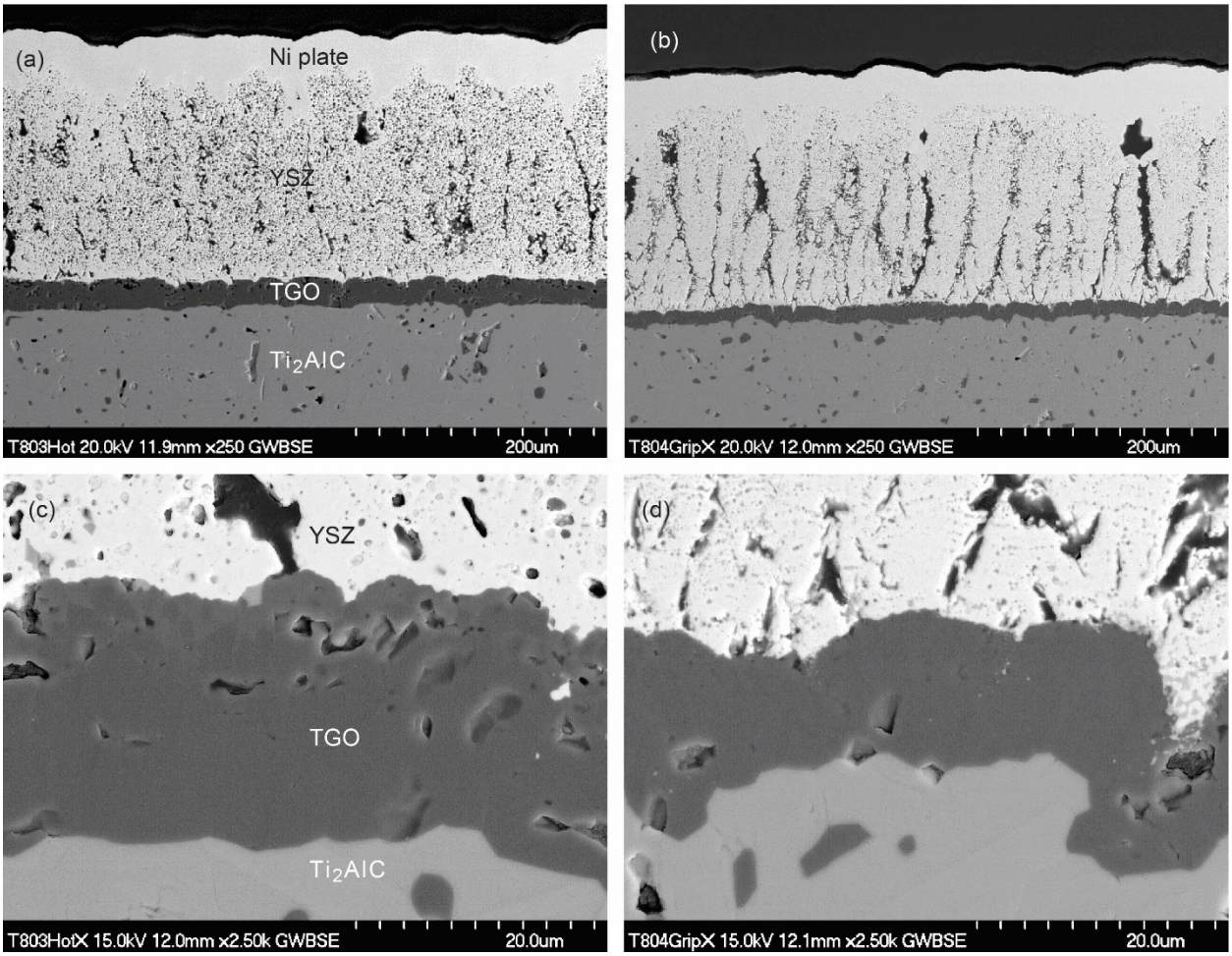

Figure 17.—BSE/SEM images of the coating face after 500 h BRT at 1300 °C. (Ni Plated) YSZ/TGO/Ti_2AlC matrix: (a), (c), at the hot zone; (b), (d), at the grip end. Clean interfacial structures; 22.2/20.7 and 12.4 μm alumina scale thickness, respectively.

Uncoated Backside

Optical micrographs in Figure 18 reveal zonal differences on the uncoated backside of the sample. The hot zone appears rather fibrous and filamentary at low magnification, and a more uniform granular structure at the top (warm zone) of the bar. Similarly, Figure 19 provides SEM images of the hot zone backside that reveal an ‘open’ structure at low magnification Figure 19(a) and unsupported protruding etched platelets at high magnification Figure 19(b). The EDS spectra show the granular regions (G) to be Al_2O_3, while the platelets (P) exhibit Ca, Ti, Mg impurities. Ti contamination is probably a remnant of

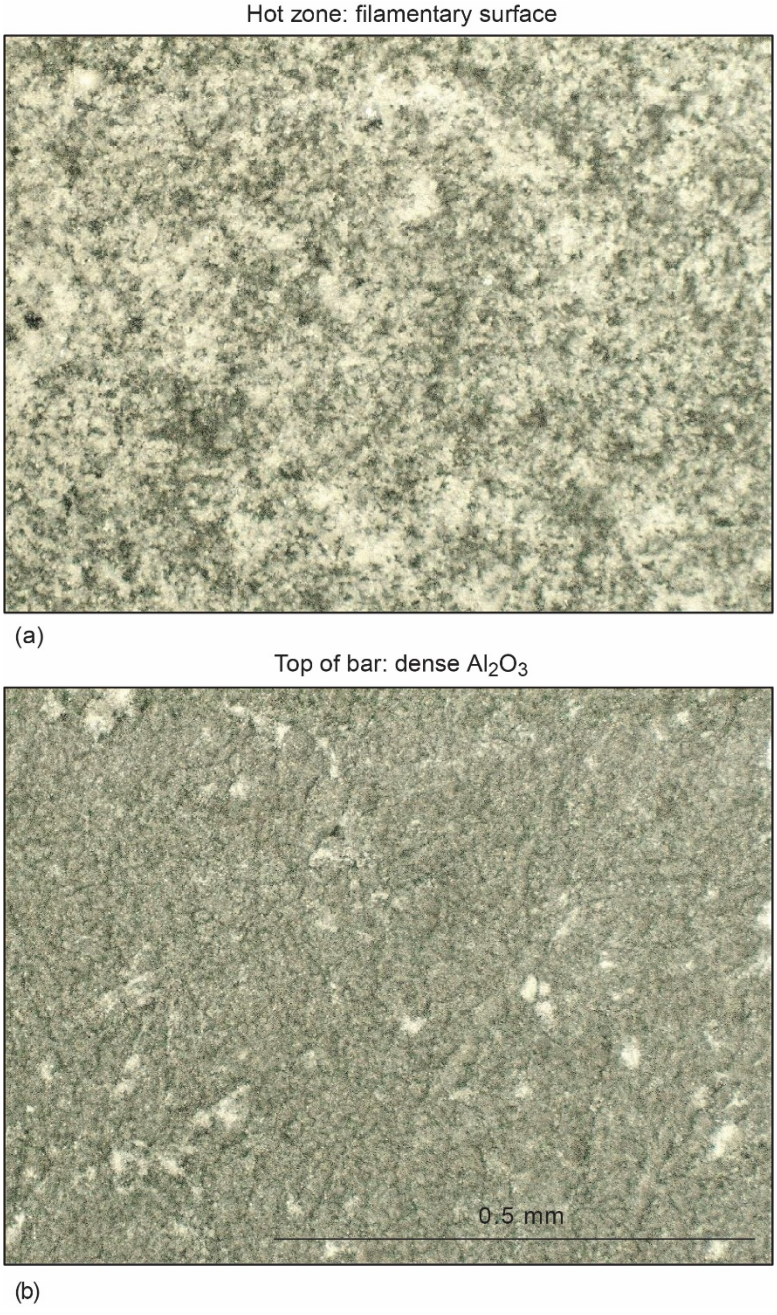

Figure 18.—Optical surface micrographs of uncoated Ti_2AlC backside after 500 h BRT at 1300 °C. (a) Nonuniform bright streaks in hot zone. (b) More uniform scale appearance at cooler top end of sample.

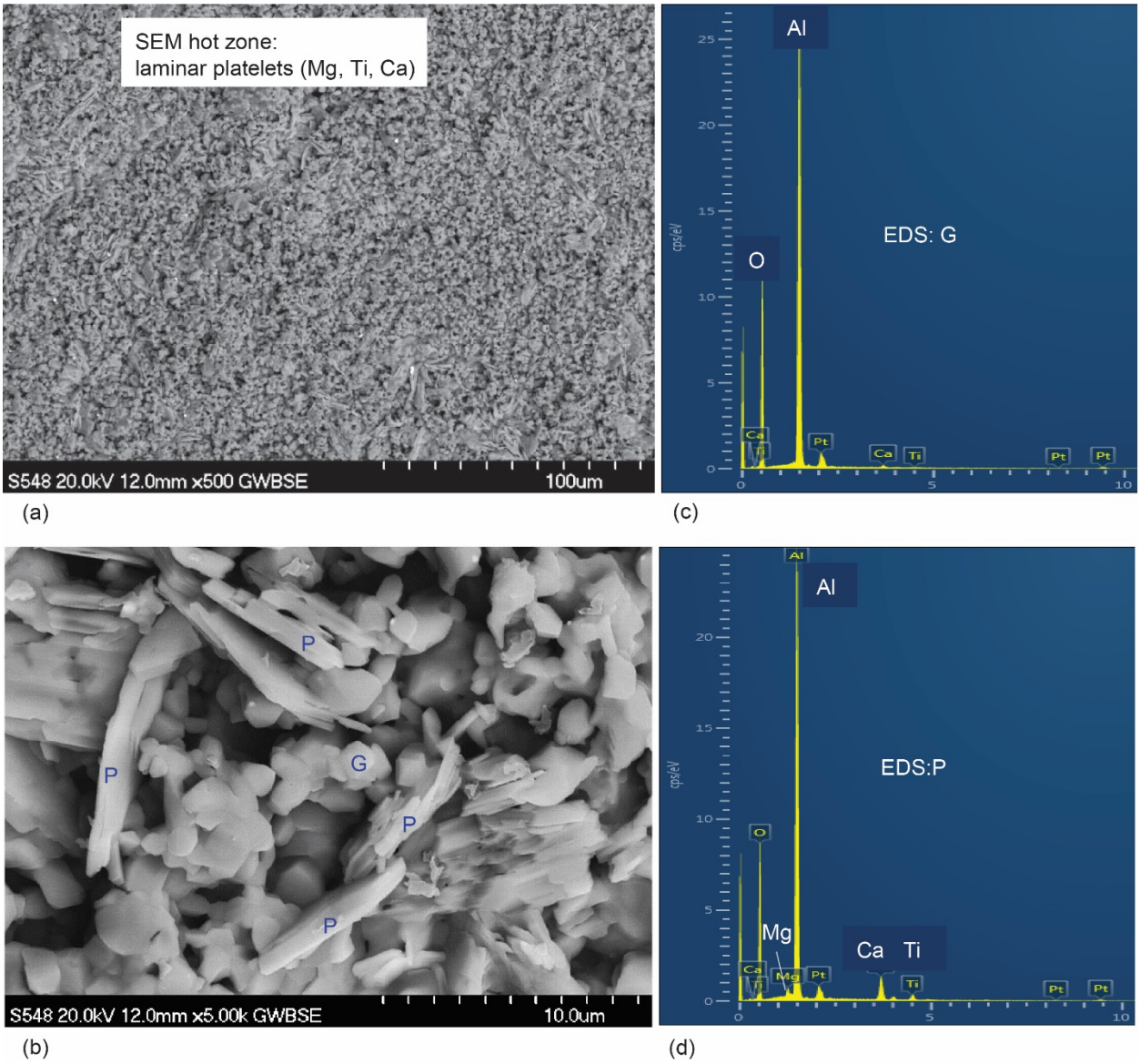

Figure 19.—SEM/BSE images of uncoated backside Ti_2AlC surface at the hot zone after BRT. (a) Textured open scale structure shown in Figure 16. (b) Higher magnification showing individual laminar ~1 x 5 μm platelets (P); corresponding EDS spectra showing: (c) High Al, O intensity for granular particle (G); (d) Small Mg, Ca, Ti peaks corresponding to platelets (P).

TiO_2 transient oxide features. $TiAl_2O_5$ and $(Ca,Mg)TiO_3$ are possible as stable reaction phases, though the nodules at 1 μm are too small to isolate their EDS response from the underlying alumina. Ca and Mg may arise from dissolved minerals in cooling water or from air supply line calcium-magnesium-alumino-silicate (CMAS) contaminants, although no Si was observed. No Ca, Mg phases were identified by xrd and little solubility exists within alumina. The faceted laminar structure is believed to be a vestige of $TiO(OH)$ or $Al(OH)_3$ volatile hydroxide formation and concomitant water vapor etching. The incorporation of impurities may indicate a role in reformation or growth of the scale. No Ca, Mg, Al, or Si EDS peaks were observed on the YSZ TBC face, only Y, Zr, and O.

By contrast, the warm top region (Figure 20) exhibits a relatively uniform granular structure, decorated by colonies of dispersed bright nodules. Again, the granular regions (G) are relatively pure Al_2O_3, while the nodules (N) contain appreciable levels of Ti and Ca. The high levels of Ti are more clearly vestiges of previous transient TiO_2 particles, while, again, Ca was likely an air supply contaminant. The granular regions exhibit grain boundary porosity that may indicate some level of etching by $Al(OH)_3$ formation. Finally, the grip end represents the coolest region of the sample (Figure 21) and shows perhaps a higher distribution of Ti, Ca-rich nodules (N) among the pure Al_2O_3 grains (G).

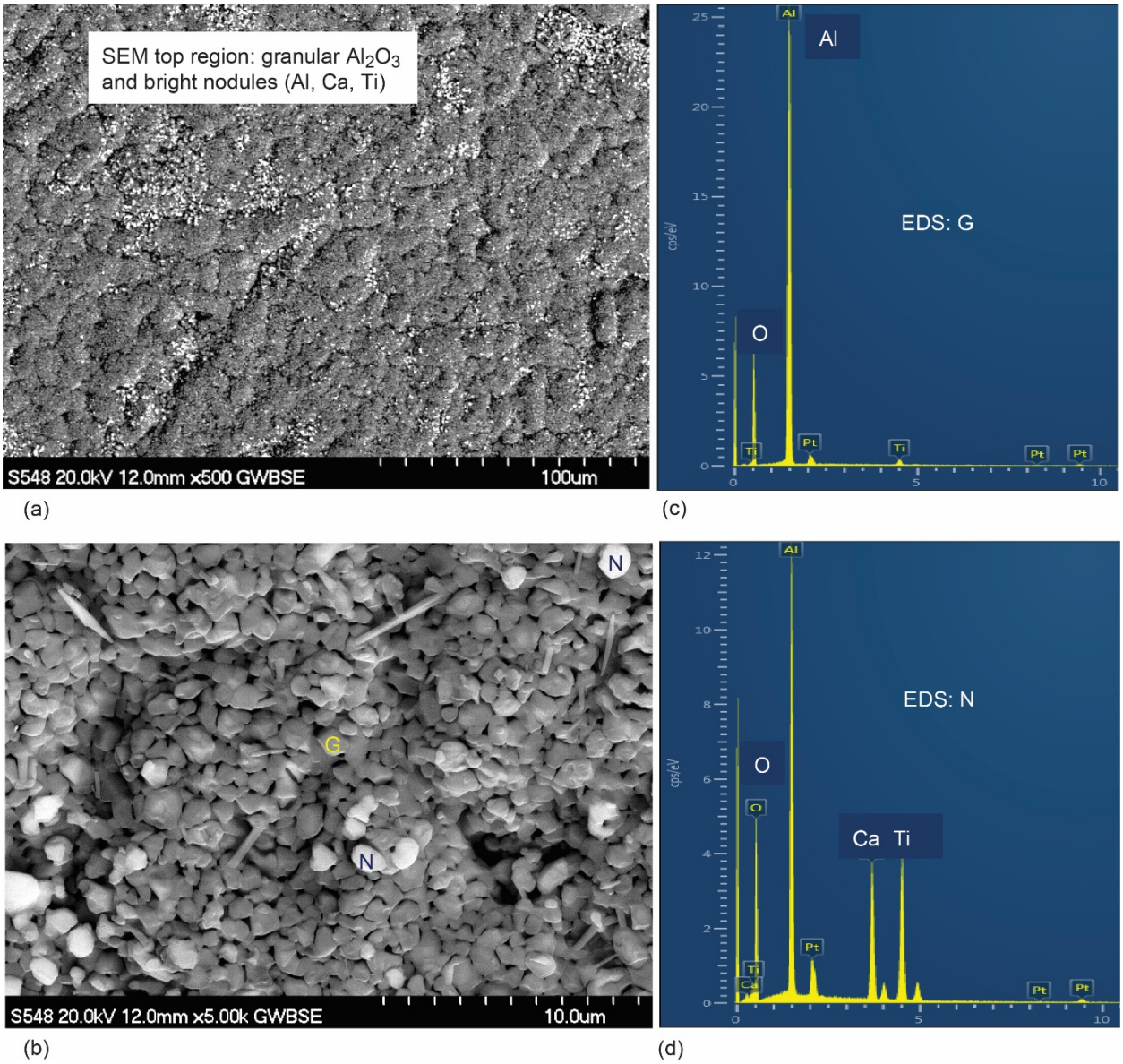

Figure 20.—SEM/BSE images of uncoated backside Ti_2AlC surface at the top end after BRT. (a) Finely peppered nodules dispersed on textured dense scale structure shown in Figure 16. (b) Higher magnification showing individual equiaxed ~1 μm grains (G) and bright nodules (N); corresponding EDS spectra showing. (c) High Al, O intensity for granular particle (G). (d) High Ca, Ti peaks for bright nodules (N).

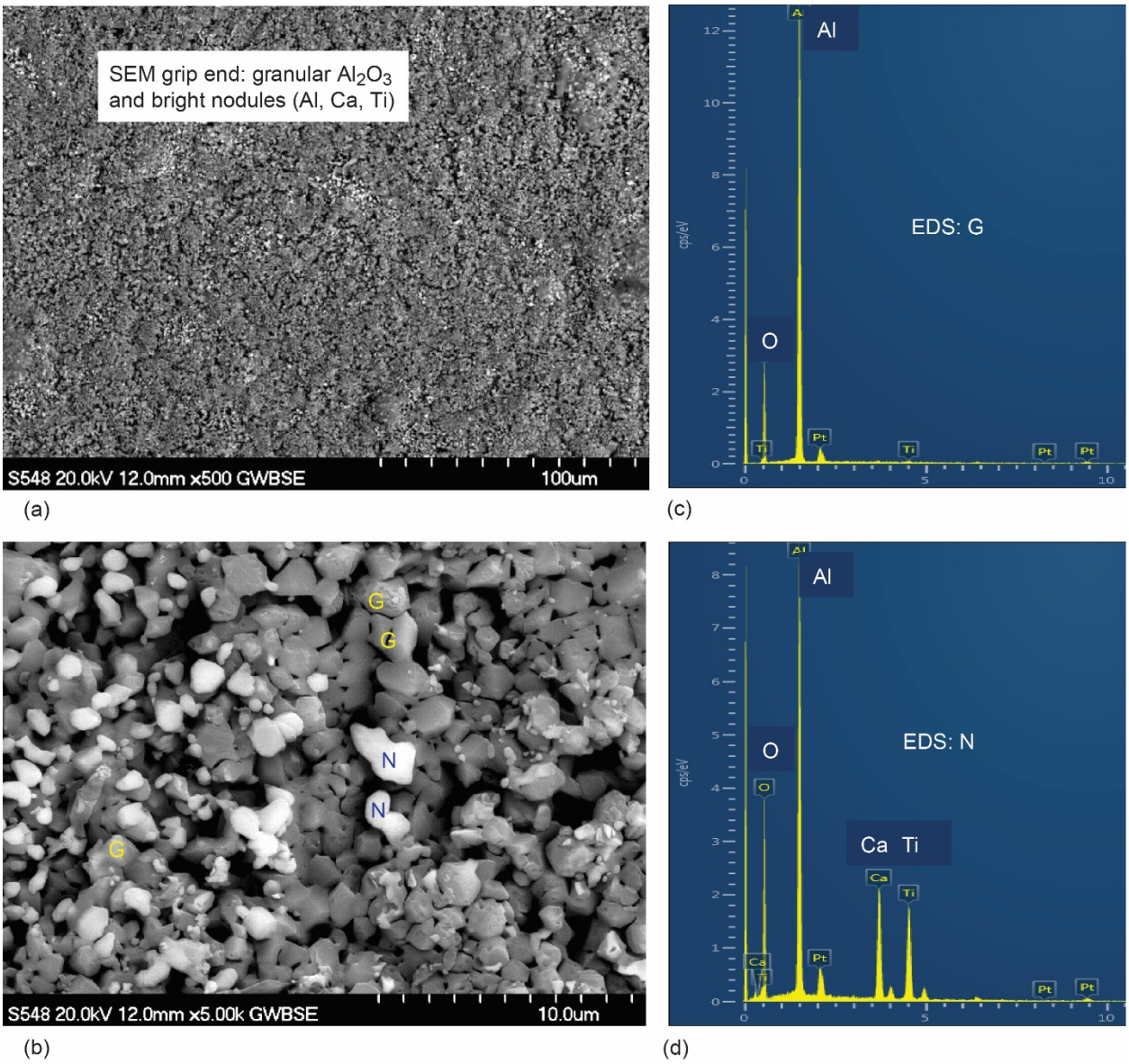

Figure 21.—SEM/BSE images of uncoated backside Ti_2AlC surface at the lower grip end after burner test. (a) Finely peppered nodules dispersed on textured dense scale structure. (b) Higher magnification showing individual equiaxed ~1 μm grains (G) and bright nodules (N); corresponding EDS spectra showing: (c) High Al, O intensity for granular particle (G). (d) Additional high Ca, Ti peaks corresponding to bright nodules (N).

Cross section optical micrographs of the uncoated backside in Figure 22 revealed an irregular scale/gas surface, possibly a vestige of moisture attack and $TiO(OH)_2$ and $Al(OH)_3$ volatile oxide formation. Here the backside scale thicknesses were approximately 14.7 and 8.2 μm thick, (12.4/13.8 and 9.0 μm SEM), respectively. The reduced scale thickness, compared to the coated front side with direct flame impingement, can therefore be attributed to both reduced backside temperature and volatility losses from the bare scale. The SEM images Figure 23 show the same features, with more detail regarding the faceted, highly convoluted, open Al_2O_3 structures formed by hydroxide volatility etching effects. The relative amount of this filamentary surface Al_2O_3 is much thicker (and more dense) for the cool grip end (68 percent, at 6.2 μm) versus the hot zone (35 percent, at 4.8 μm), i.e., volatility effects (surface removal) and oxidation (inward layer growth) are expected to be greater for the higher temperatures in the hot zone.

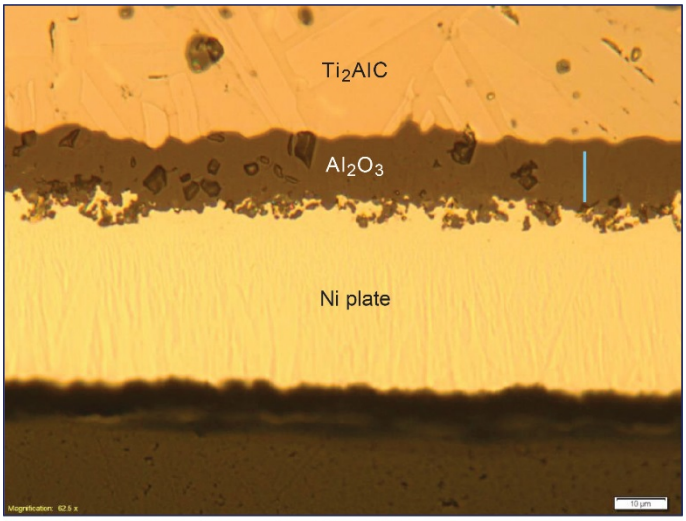

(a) Hot zone
14.7 μm TGO

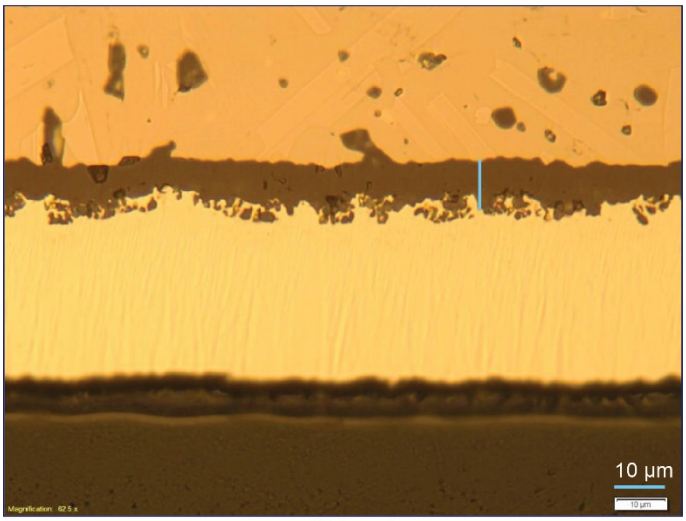

(b) Grip end
8.2 μm TGO

Figure 22.—Ti_2AlC backside optical micrographs; polished cross sections after 500 h BRT at 1300 °C (Ni-plated). (a) Hot zone, 14.7 μm thick alumina scale. (b) Cooler grip end, 8.2 μm thick alumina scale.

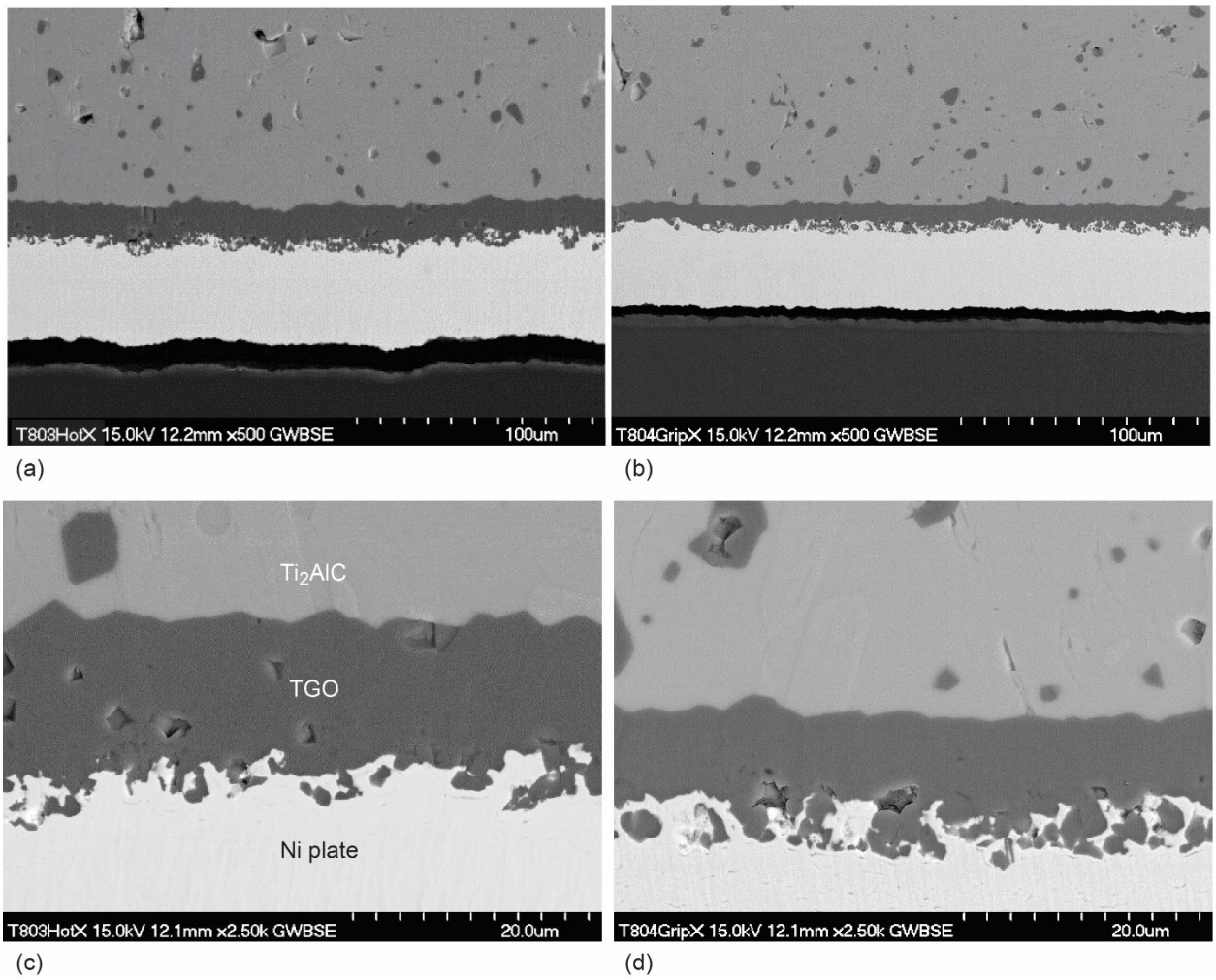

Figure 23.—BSE/SEM images of the uncoated backside after 500 h BRT at 1300 °C. (Ni Plated) TGO/Ti_2AlC matrix: (a), (c), at the hot zone; (b), (d), at the grip end. Clean interfacial structures with moisture attack of external scale; 12.4/13.8 and 9.0 μm alumina scale thickness at hot zone and grip end, respectively.

The oxygen weight gains for various scale thicknesses can be projected by the 3.99 g/cm^3 density of Al_2O_3, i.e., by dividing the thickness by 5.339 μm/(mg/cm^2). The weight changes of ~(4.1, 2.6) mg/cm^2 are thus indicated for scales corresponding to the hot zone, (face, backside) at ~(22, 14) μm, and ~(2.2, 1.7) mg/cm^2 corresponding to the grip end (face, backside) at ~(12, 9) μm. Recall that corresponding reductions in specific weight gain are expected for cooler portions of the strip sample because the exposed length (50 mm) was about twice the diameter of the exit nozzle (25 mm) impinging hot gas stream. The actual measured weight gain was in the midrange at 2.4 mg/cm^2, i.e., near the projected 2.7 mg/cm^2 averaged over both Ti_2AlC faces (projected hot zone at ~1244 °C and measured backside at 1216 °C, respectively), plus the vertical thermal gradients.

X-ray Diffraction and Raman

Xrd diffractometer scans of the back (bare) and front (coated) phases are shown in Figure 24. They correspond to positions along the length for samples exposed briefly at 926 °C (S1) and long term at 1300 °C (S2). It first noted that the uncoated backside phases corresponding to the previous microstructures have identified α-Al_2O_3 as the principal scale phase. The 211 MAX phase structure (M) was also

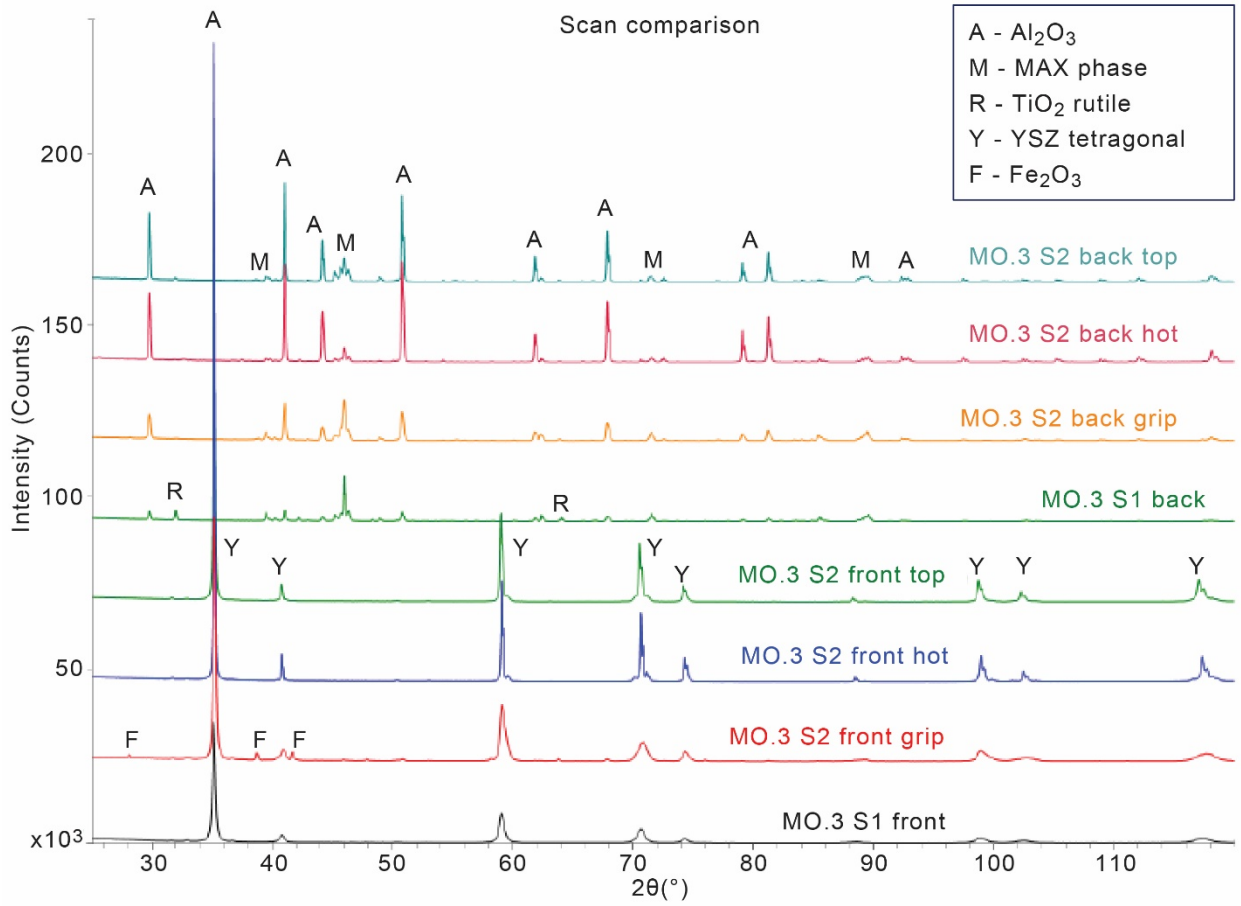

Figure 24.—A comparison of XRD scans for uncoated and YSZ coated sides for the Ti_2AlC burner sample tested at 926 °C for 10 m (S1), then at 1300 °C for 500 h (S2). Hot zone, top end, and grip end positions. Primary peaks for (A) α-Al_2O_3, (R)TiO_2 rutile, (M) Ti_2AlC MAX phase, (Y) cubic/tetragonal YSZ, and (F) Fe_2O_3 hematite.

identified. TiO_2 rutile (R) was mainly evident for the short initial exposures (10 min.). Secondly, the YSZ phases on the front coated surface indicate primarily overlapping tetragonal and cubic structures (Y), with a minor level of Fe-oxide (F) from grip end contamination. These are now discussed in more detail.

Table 1 lists the estimated wt% of phases identified in Figure 24 calculated by Rietveld whole pattern fitting. The first part of the table corresponds to the scale phases formed on the uncoated backside. The first entry corresponds to the burner slab exposed up to 926 °C for only a few minutes when a leading-edge crack was observed (the burner was then immediately shut down). The remainder of the entries correspond to various positions after 1300 °C testing. α-Al_2O_3 became very dominant in the hot zone, here (97 percent), the MAX phase was still evident (3 percent), but TiO_2 was just a very weak trace (0.1 percent). This is indicative of a strong tendency for initial TiO_2 transients to become greatly diminished with respect to the steady state α-Al_2O_3 growth. It is also consistent with preferential vaporization removal in water vapor as $TiO(OH)_2$ compared to $Al(OH)_3$ losses (Figure 19 to Figure 21). A small amount of substrate $TiAl_3$ may have been possible, but very tentative due to overlapping peaks with MAX phases.

The second part of Table 1 summarizes phases observed on the YSZ coating front side. The first entry (low temperature and short time) should reflect nearly an as-coated value, i.e., a high level of the as-sprayed metastable t' tetragonal phase, balance cubic, with a trace of monoclinic. The second entry corresponds to previous long term, consecutive furnace exposures, lasting 500 h each at 1100 to 1300 °C, in 50 °C increments (2500 h total) (Ref. 13). This produced a large amount of monoclinic, with no residual t'. The third grouping was for the 1200 °C Mach 0.3 shakedown test for 500 h performed prior to the present study. A high cubic level again resulted, but a 'transformable' tetragonal made up the residual. It is not clear why this low-Y tetragonal (2 to 5 wt%) did not transform to monoclinic upon cooldown. (The $\%YO_{1.5}$ mole% was estimated for the YSZ phases by lattice parameter or c/a ratio empirical correlations, Table 2) (Refs. 29 to 32).

TABLE 1.—SUMMARY OF SURFACE PHASES FOR BURNER RIG EXPOSURE OF BARE AND YSZ COATED Ti_2ALC MAX PHASE. RIETVELD ESTIMATES OF WT% PHASE CONTENTS. TEST TEMPERATURE INDICATES MAXIMUM SURFACE TEMPERATURE OF COATING IN HOT ZONE
[Sample from previous furnace tests included for comparison.]

Request	Back, uncoated	Location	Test temperature, °C	Time	Al_2O_3	TiO_2	Ti_2AlC[a]	$TiAl_3$ (?)	Fe_2O_3[b]
08163	Burner bar	Hot zone	926	10 m	51	10	38	----	----
08142	Burner bar	Top end	1300	500 h	89	1	9	1.5	----
--------	Burner bar	Hot zone	1300	500 h	97	0.1	3	0	----
--------	Burner bar	Grip end	1300	500 h	79	0.3	17	3.5	1

Request	Front, coated	Location	Test temperature, °C	Time	t-YSZ	t'-YSZ	Cubic	Monoclinic	Fe_2O_3[b]
08021	Furnace sample	Uniform	1100 to 1300	2500 h	---	---	62	21	---
08163	Burner bar	Hot zone	926	10 m	---	68	28	3	---
08142	Burner bar	Top end	1200	500 h	34	---	62	---	---
-------	Burner bar	Hot zone	1200	500 h	31	---	64	---	---
-------	Burner bar	Grip end	1200	500 h	28	---	68	---	---
08142	Burner bar	Top end	1300	500 h	12	---	86	0.5	---
-------	Burner bar	Hot zone	1300	500 h	11	---	86	0.5	---
-------	Burner bar	Grip end	1300	500 h	---	49	32	1.5	16

[a]Includes other possible MAX stoichiometries
[b]Includes other possible Fe-oxides

TABLE 2.—ESTIMATES OF $YO_{1.5}$ MOLE% IN YSZ PHASES ACCORDING TO PUBLISHED LATTICE PARAMETER AND C/A RATIO CALIBRATIONS

					t-YSZ		t'-YSZ		cubic
	Sample	Location	Test temperature, °C	Time	*a-LP*[a]	*c/a ratio*[b]	*a-LP*[a]	c/a ratio[b]	*a-LP*[a]
08021	Furnace	Uniform	1100 to 1300	2500 h	---	---	----	----	12
08163	Burner bar	Hot zone	926	17 m	---	---	11.6	9.8	----
08142	Burner bar	Top end	1200	500 h	3.7	3.6	----	----	16.4
--------	Burner bar	Hot zone	1200	500 h	3.1	3.7	----	----	14.7
--------	Burner bar	grip end	1200	500 h	4.8	4.6	----	----	16.1
08142	burner bar	top end	1300	500 h	3.2	3.6	----	----	15.1
--------	burner bar	hot zone	1300	500 h	1.6	3.0	----	----	9.4
--------	burner bar	grip end	1300	500 h	---	---	7.0	6.8	10.9

[a]Value based on empirical correlation between mol% $YO_{1.5}$ and a lattice parameter.
[b]Value based on empirical correlation between mol% $YO_{1.5}$ and c/a ratio. See report narrative for discussion of t' vs. t phases.

The highest material temperature corresponds to the middle hot zone, with a ‘warm’ top of the bar and ‘cool’ grip end bottom. Similarly for the 1300 °C test here, a very high level of cubic resulted. The cool grip end showed a large amount of high Y (7 wt%) tetragonal. Surprisingly, none of the burner rig samples exhibited high levels of monoclinic. It should be mentioned that while Rietveld analyses were used, long exposures at high angles were not specifically targeted to maximize resolution. Thus, peak deconvolution and phase distinctions may entail some ambiguity.

Typically, aged YSZ will phase separate into low Y tetragonal (and monoclinic) and high Y cubic phases at their respective ends of the tie line, e.g., as did the 2500 h furnace sample. The high cubic contents for the 1200 °C 500 h burner sample is consistent with this projection. However, the low Y tetragonal unexpectedly did not transform to monoclinic. Furthermore the 1300 °C 500 h burner sample became primarily cubic with neither tetragonal phase and little monoclinic. One might suspect a compositional change specific to burner exposures. It is well known that combusted jet fuel contains ~10 percent water vapor and that moisture can have a Y-leaching effect on YSZ. Y-leaching compositional changes would be inconsistent with the large amounts of Y-rich cubic phases in these burner samples. Further insights and comparisons are available in the recent PS-PVD phase stability study that did show transformation to monoclinic more readily (Ref. 28).

Some preferred deposition growth orientation (fiber texture) of the YSZ columns was observed, as indicated by the inverse pole figures of Figure 25. The strongest orientation was for $(111)_{flourite}$, with a secondary weak orientation of $(200)_{flourite}$.

While monoclinic appears to be missing in many cases from the XRD results, Raman analyses (Figure 26) were able to discern small peaks for monoclinic in PS-PVD samples produced at the same time and with typical wavenumbers, marked ‘M,’ and tetragonal peaks marked ‘t’. These corresponded in general to peaks noted in a study of bulk YSZ (Ref. 33). It is also noted that monoclinic may not appear instantaneously upon cooling, but require additional stress (grinding APS YSZ) (Ref. 34) or some time interval of nucleation for ‘isothermal’ martensite to appear at room temperature (in EB-PVD YSZ after aging at 1425 °C) (Ref. 35). The retention of metastable phases versus instantaneous martensite is a well-known phenomenon where the compensating shear associated with transformation lathes and twins must overcome mechanical constraints, such as fine grain size. The PS-PVD YSZ and both TGO interfaces in this study are being studied in a subsequent FIB-STEM investigation.

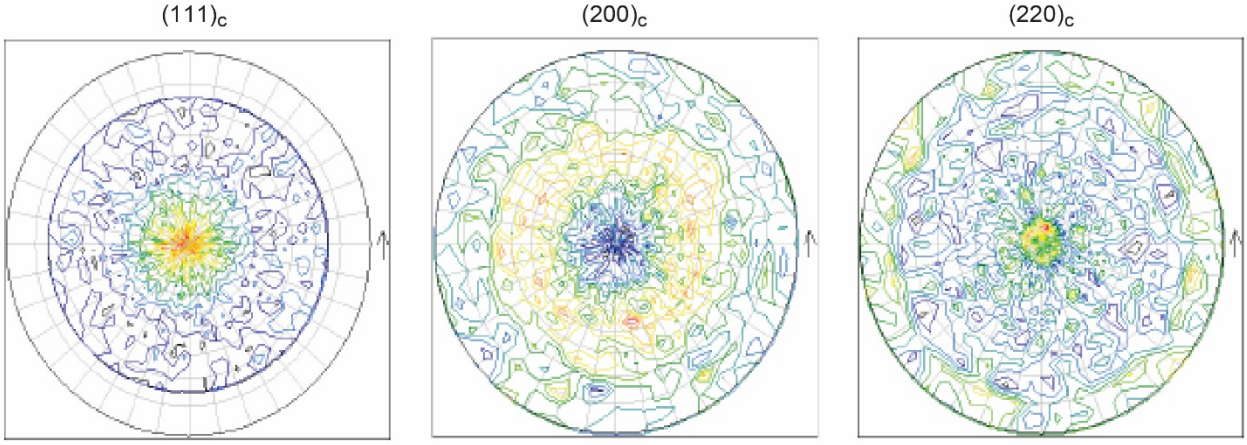

Figure 25.—Pole figures from YSZ columns showing primarily a (111) fiber texture (926 °C/10 m exposure). BGYR color scale corresponds to relative intensity range. (a) $(111)_{cubic}$ 200 to 450 range. (b) $(200)_{cubic}$, 0.5 to 1.6 range. (c) $(220)_{cubic}$, 0.8 to 1.5 range.

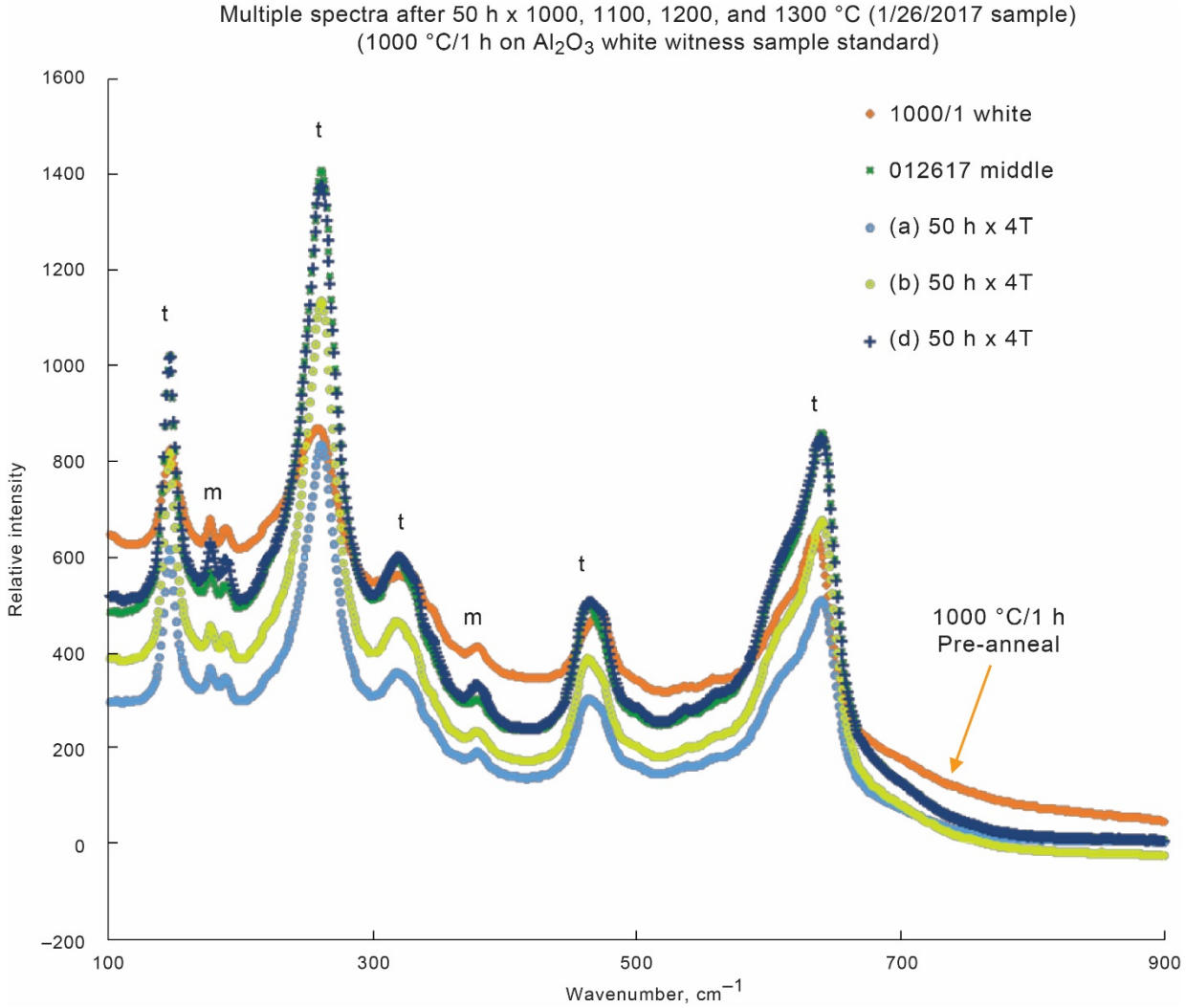

Figure 26.—Raman spectra of PS-PVD coatings indicating 178, 190, 381 cm^{-1} peaks typically associated with monoclinic (M) YSZ and 142, 258, 322, 467, and 637 cm^{-1} associated with tetragonal (Ref. 33). Annealed at 1000 °C/1 h (white, Al_2O_3 substrate) and four duplicate spectra for YSZ aged 50 h each at 1000, 1100, 1200, and 1300 °C, successively.

Discussion of Durability and Volatility

The exceptional durability of this Ti_2AlC-TBC system has again been demonstrated, but now under more extreme environmental conditions. Its success was due to beneficial matching of thermal expansion coefficients between the YSZ top coat, Al_2O_3 TGO, and Ti_2AlC substrate (~11.7, 9.3, and 10.2×10^{-6}/K) combined with the excellent oxidation resistance of Al-MAX phases. The present test provided the added factors of long term, high velocity (100 m/s) moisture attack and thermal shock compared to the previous furnace tests.

In our related burner studies, bare Ti_2AlC had also been shown to survive oxidation, moisture-induced recession (scale volatility), and thermal shock in 50 h high pressure burner rig (HPBR) exposures up to 1300 °C (Ref. 11). That data, shown in Figure 11, is similar to the present data, but necessarily of much shorter duration because of the complexity of that rig. The HPBR test (6 atm., 25 m/s) produced moderate weight gains or slight losses (~0.01 mg/cm^2h) when pre-oxidized, indicating only slight temporary scale volatility in water vapor.

Data from both burner tests produced less oxidation than both furnace tests - no volatility occurs at the low H_2O content and low gas velocity in the furnace tests. It is generally agreed that Al_2O_3 growth on Ti_2AlC occurs by grain boundary diffusion of oxygen through the scale (Refs. 3 and 36). Coupled with nearly cubic grain growth, this results in sub-parabolic cubic scale growth. The weight gain kinetics of the Mach 0.3 test were therefore analyzed in a manner similar to the TGA and HPBR studies (Refs. 11 and 37). The good fit to $t^{1/3}$ cubic kinetics produced $k_c = 0.012$ mg^3/cm^{6}h, lower than the TGA and HPBR results of 0.200 and 0.024 mg^3/cm^{6}h, respectively.

This implies that the burner test exhibited less scale growth due to three factors: 1) reduced temperature due to thermal gradients from the central hot TBC impingement face to the ends and bare backside; 2) volatility of TiO_2 and Al_2O_3 scales from the bare backside from high velocity water vapor (via $TiO(OH)_2$ and $Al(OH)_3$, in that order); and 3) reduced transient TiO_2 formed during low pressure PS-PVD deposition. Therefore, precise mechanistic assessments of weight change are difficult for these Mach 0.3 results, with one side coated and substantial thermal gradients.

The bare backside was measured as 1216 °C (2220 °F). (Heat transfer calculations arrived at 1204 °C backside and 1244 °C for the front side YSZ-Ti_2AlC interface temperatures). (For the preliminary uncoated slab, face-on test, the backside was measured only 10 °C lower than the front face). From the cross-sections, the TGO under the coating at the grip end was found to be~1/2 that in the hot zone. It can then be shown, using the cubic oxidation law, that $k_{hot} \approx 8\ k_{grip}$. The interface temperature was estimated as 1244 °C. Using the Arrhenius relation from Ti_2AlC kinetics (Ref. 37), this corresponds to 1134 °C, or about 100 °C cooler at this section just above (~1 mm) the grip end.

For the uncoated backside, the high velocity of the atmospheric Mach 0.3 test (1 atm., 100 m/s) may be as important as the high-pressure environment of the HPBR. Note that volatility losses vary as $v^{1/2}$. Thus a 2× increased volatility rate is projected for the Mach 0.3 test due to 4× velocity (100 m/s vs. 25 m/s). Volatility should also scale as $p_{H2O}/p_{tot}^{1/2}$ for TiO_2 scales, $p_{H2O}^{3/2}/p_{tot}^{1/2}$ for Al_2O_3, and $p_{H2O}^{2}/p_{tot}^{1/2}$ for SiO_2, predicated on $TiO(OH)_2$, $Al(OH)_3$, and $Si(OH)_4$ volatile species (Refs. 8 to 10). Given that the moisture content of combusted jet fuel is ~10 percent, the predicted loss rate relative to the HPBR test can be projected as 0.82, 0.33, and 0.14 for TiO_2, Al_2O_3, and SiO_2 scales, respectively, as listed in Table 3. The similarity of Mach 0.3 to HPBR data is consistent with primarily TiO_2 losses, i.e., a volatility loss ratio near unity. The microstructural results again indicated substantial removal of surface TiO_2, with etching of Al_2O_3 grains, in qualitative agreement with expectations.

TABLE 3.—TYPICAL HPBR AND MACH 0.3. (a) BURNER CONDITIONS. (b) RELATIVE SCALE VOLATILITY FACTORS ($J_{M0.3}/J_{HPBR}$) ACCORDING TO $v^{1/2}p_{H20}{}^{n}/p_{tot}^{1/2}$

(a)

	$v\,(m/s)$	$P_{H20}\,(atm)$	$P_{tot}\,(atm)$
Mach 0.3	100	0.1	1
HPBR	25	0.6	6

(b)

Scale	Species	n	$(P_{H20}/P_{H20})^{n}$	$(P_{tot}/P_{tot})^{1/2}$	$(v/v)^{1/2}$	$J_{Mach\ 0.3}/J_{HPBR}$
TiO_2	$TiO(OH)_2$	1	0.167	0.408	2	0.816
Al_2O_3	$Al(OH)_3$	3/2	0.068	0.408	2	0.333
SiO_2	$Si(OH)_4$	2	0.028	0.408	2	0.136

Figure 11 also presents similar Mach 0.3 tests of a 'Hexoloy' monolithic sintered SiC standard baseline material for nominally duplicate atmospheric BRT runs, a, b, c, showing weight losses of –1.2, –2.8, and –6.6 mg/cm^2 after 200 h (Ref. 20). The weight loss for SiO_2 scales is from $Si(OH)_4$, where the projected Mach 0.3 BRT loss rate is only 0.14 that for the HP-BRT volatility rates, i.e., according to $v^{1/2} \times (p_{H2O})^2/p_{tot}^{1/2}$. Thus, pressure effects are emphasized for SiC substrates, while velocity effects are pronounced for TiO_2. High pressure water vapor was shown in HP-BRT to be particularly more detrimental for SiC (Ref. 20). The HP-BRT curve shown in Figure 11 was interpolated from Equation (2) (Ref. 38). Indeed, the SiC loss rate calculated for the Mach 0.3 BRT relative to the HP-BRT results was estimated to be 0.136, giving –1.14 mg/cm^2 after 100 h, close to the actual –1.00 mg/cm^2 given by experimental curve 'b'.

The resistance of YSZ and Ti_2AlC to oxide volatility compared to SiC is clearly shown in Figure 11. Comparison of the rig and furnace data indicate lower weight gains produced by burner tests due in part to volatility losses. The similarity of HPBR and Mach 0.3 results are more consistent with TiO_2 losses. However, Jacobson predicted higher vapor pressures and loss rates for Al_2O_3 than TiO_2 in water vapor using thermodynamic data (Ref. 11). SiO_2 scales, on the other hand, were rapidly removed, showing substantial losses in both tests and more pronounced pressure sensitivity compared to velocity as predicted (Ref. 8). SiO_2 scales have been shown to oxidize by paralinear kinetics in water vapor (Ref. 17). There has been some suggestion that the Ti_2AlC oxidation kinetics in BRT can be treated by a cubic-linear law, but the present test configuration complicates such analysis.

Long term YSZ TBC/Ti_2AlC MAX phase oxidative compatibility had been shown in successive 1100 to 1300 °C interrupted furnace tests for a total of 2500 h (Ref. 13**)**. Based on TGO scale thickness, this was equivalent to a TBC oxidative life of 25 to 50× that determined for conventional single crystal superalloys. The present Mach 0.3 TBC-MAX survival can be similarly compared, as summarized in Table 4. TBCs on superalloys survive on average only 30 h at 1280 °C, or, alternatively, 500 h at 1150 °C (Ref. 15). An advanced two-layer Gd_2Zr_2O7-YSZ coating was shown to survive 588 1-h cycles at 1100 °C and 42 hot hours with a surface temperature of 1400 °C in a gradient burner test (Ref. 39).

TABLE 4.—LIFE (h) SUMMARY OF YSZ TBC ON MAX PHASES COMPARED TO SUPERALLOYS (SXSA, REF. 15; GZ/YSZ, REF. 39; FCT KANTHAL (K) REFS. 13, 40; FCT, BRT JUELICH (J), REFS. 14, 25)

Test	TBC	Substrate	**1100°**	**1150°**	**1200°**	**1250°**	**1300°**	**1400°**	°C
FCT	PVD	SXSA	*831*	*352*	*158*	*75*	*37*		h
FCT	HVAF[a]	Hast-X	*580*						
BRT	**HVAF[a]**	**IN-738**						***42***	
FCT	APS	Cr_2AlC-K	500	500	*100*				
FCT	PS-PVD	Cr_2AlC-K	500	500	*100*				
FCT	APS	Cr_2AlC-J	500		500		*268*		
BRT	**HV-APS**	**Cr_2AlC-J**						***62***	
FCT	APS	Ti_2AlC-K	500	500	500	500	*500*		
FCT	PS-PVD	Ti_2AlC-K	500	500	500	500	500		
BRT	**PS-PVD**	**Ti_2AlC-K**			**500**		**500**		

[a]2-layer $Gd_2Zr_2O_7$/YSZ (Ref. 39)
K-Kanthal (Refs. 15, 13, and 40)
J-Juelich (Refs. 14 and 25)
Black-survived
Red-failed

APS YSZ coatings have been shown to survive 500 h up to 1200 °C on high purity Cr_2AlC(-Juelich) MAX phase or to 268 h at 1300 °C (Ref. 14). Commercial purity Cr_2AlC(-Kanthal) MAX phase substrates exhibited failure in stepped, interrupted furnace tests beginning at 400 h at 1150 °C, and complete after 100 h at 1200 °C (Refs. 40 and 27). While Cr_7C_3 depletion layers and impurities have generally been associated with scale/TBC spallation, interfacial delamination was also observed, unlike Ti_2AlC MAX phase that exhibits no depletion zone or scale adherence issues. The high gradient BRT test using Cr_2AlC as a bond coat survived 745 fast heating cycles (5 min.), with a high TBC surface temperature of 1400 °C but low TGO interface temperature of 1050 °C (Ref. 25). Again, a porous Cr_7C_3 depletion layer, now exacerbated by Al interdiffusional losses for Cr_2AlC as a bond coat, was detrimental to the coating system.

The improved lifetime durability of YSZ/MAX phases was presented as scale thickness versus temperature, where TGO scales upwards of 30 to 40 μm were sustained compared to 5 to 10 μm for single crystal superalloys (Ref. 14). Alternatively, the life duration versus temperature is presented in Table 4. It can be seen that TBCs on MAX phases survive to higher temperatures and at hundreds of hours above 1200 °C, with an overall time advantage for Ti_2AlC substrates compared to Cr_2AlC. The BRT test of the present study supports this trend, with no sign of failure after 500 h at either 1200 °C or 1300 °C.

The cyclic durability of YSZ on SiC is improved with specialized bond coats, but still quite limited because of thermal expansion incompatibility (Refs. 41 and 42). However, note that $Yb_2Si_2O_7$ EBC coatings have been engineered for protecting strong SiC CMC materials in high temperature water vapor. It was also shown that Al_2O_3-containing additives can dramatically reduce moisture-assisted oxidation under the EBC (Ref. 43). These systems typically survive 1000 h furnace exposures in high water vapor contents at 1316 °C, while also exhibiting low volatility rates in moving gases (Refs. 21 to 23). The overall durability of EBCs for CMCs in aggressive turbine environments at temperatures ≥ 1300 °C remains a topic of great importance and interest.

Conclusions

The durability of a PS-PVD YSZ coating on a Ti_2AlC MAX phase substrate has been demonstrated by cyclic 500-h Mach 0.3 burner rig testing at 1300 °C. No spalling or visible degradation of the coating occurred. This represents perhaps the longest TBC survival duration in an aggressive 1300 °C burner rig test. The modest weight gain due to protective α-Al_2O_3 scale growth was not life limiting. Oxidative life benefited from the CTE matching of substrate, TGO, and TBC. The YSZ face coating showed no evidence of oxide volatility or reactivity with moisture. Xrd indicated some as-deposited texture, an increase in the amount of cubic phase with thermal exposure, but no indication of massive monoclinic destabilization products. Moderate bending of the Ti_2AlC sample, however, was indicative of creep and low strength at high temperature.

Comparisons with uncoated Ti_2AlC 1300 °C furnace and high-pressure burner data indicate similar cubic growth behavior, with lower values observed for rig tests. Surface SEM of the uncoated backside showed effective removal of TiO_2 surface nodules possibly via $TiO(OH)_2$, with crystallographic etching of Al_2O_3 grains presumably via $Al(OH)_3$. In contrast, SiC exhibited notable weight loss from $Si(OH)_4$ under similar Mach 0.3 atmospheric conditions, becoming more severe at high pressures.

References

1. M.W. Barsoum and M. Radovic, “Elastic and Mechanical Properties of the MAX Phases,” Annu. Rev. Mater. Res., vol. 41, no. 1, pp. 195–227, 2011.
2. M. Radovic and M.W. Barsoum, “MAX phases: Bridging the gap between metals and ceramics,” Am. Ceram. Soc. Bull., vol. 92, no. 3 April, pp. 20–27, 2013.
3. D.J. Tallman, B. Anasori, and M.W. Barsoum, “A Critical Review of the Oxidation of Ti_2AlC, Ti_3AlC_2 and Cr_2AlC in Air,” Mater. Res. Lett., vol. 1, no. 3, pp. 115–125, Sep. 2013.
4. X.K. Qian, X.D. He, Y.B. Li, Y. Sun, H. Li, and D.L. Xu, “Cyclic oxidation of Ti_3AlC_2 at 1000–1300 °C in air,” Corros. Sci., vol. 53, pp. 290–295, 2011.
5. N.S. Jacobson et al., “Performance of Ceramics in Severe Environments,” vol. 5245, pp. 1–14, 2005.
6. S. Basu, N. Obando, A. Gowdy, I. Karaman, and M. Radovic, “Long-Term Oxidation of Ti_2AlC in Air and Water Vapor at 1000–1300 °C Temperature Range,” J. Electrochem. Soc., vol. 159, no. 2, p. C90, 2012.
7. N. Jacobson, D. Myers, E. Opila, and E. Copland, “Interactions of water vapor with oxides at elevated temperatures,” in Journal of Physics and Chemistry of Solids, 2005, vol. 66, no. 2–4, pp. 471–478.
8. E.J. Opila, N.S. Jacobson, D.L. Myers, and E.H. Copland, “Predicting Oxide Stability in High-Temperature Water Vapor,” JOM, no. January, pp. 22–27, 2006.
9. E.J. Opila and D.L. Myers, “Alumina Volatility in Water Vapor at Elevated Temperatures,” J. Am. Ceram. Soc., vol. 87, no. 9, pp. 1701–1705, 2004.
10. Q.N. Nguyen, D.L. Myers, N.S. Jacobson, and E.J. Opila, “Experimental and Theoretical Study of Thermodynamics of the Reaction of Titania and Water at High Temperatures; NASA/TM—2014-218372,” Cleveland, OH, 2014.
11. J.L. Smialek, “Environmental resistance of a Ti_2AlC-type MAX phase in a high pressure burner rig,” J. Eur. Ceram. Soc., vol. 37, no. 1, pp. 23–34, 2017.
12. J. Gonzalez-Julian, T. Go, D.E. Mack, and R. Vaßen, “Environmental resistance of Cr_2AlC MAX phase under thermal gradient loading using a burner rig,” J. Am. Ceram. Soc., vol. 101, no. 5, pp. 1841–1846, May 2018.
13. J.L. Smialek, B.J. Harder, and A. Garg, “Oxidative durability of TBCs on Ti_2AlC MAX phase substrates,” Surf. Coatings Technol., vol. 285, no. 1, pp. 77–86, 2016.
14. J. Gonzalez-Julian, T. Go, D.E. Mack, and R. Vaßen, “Thermal cycling testing of TBCs on Cr_2AlC MAX phase substrates,” Surf. Coatings Technol., vol. 340, no. November 2017, pp. 17–24, 2018.
15. J.L. Smialek, “Compiled furnace cyclic lives of EB-PVD thermal barrier coatings,” Surf. Coat. Technol., vol. 276, pp. 31–38, 2015.
16. E.J. Opila, J.L. Smialek, R.C. Robinson, D.S. Fox, and N.S. Jacobson, “SiC Recession Caused by SiO_2 Scale Volatility under Combustion Conditions: II, Thermodynamics and Gaseous Diffusion Model,” J. Am. Ceram. Soc., vol. 82, no. 7, pp. 1826–1834, 1999.
17. E.J. Opila and R.E. Hann, “Paralinear Oxidation of CVD SiC in Water Vapor,” J. Am. Ceram. Soc., vol. 80, no. 4, pp. 197–205, 1997.
18. E.J. Opila, “Volatility of Common Protective Oxides in High-Temperature Water Vapor: Current Understanding and Unanswered Questions,” Mater. Sci. Forum, vol. 461–464, pp. 765–774, 2004.
19. P.J. Meschter, E.J. Opila, and N.S. Jacobson, “Water Vapor–Mediated Volatilization of High-Temperature Materials,” Annu. Rev. Mater. Res., vol. 43, no. 1, pp. 559–588, Jul. 2013.
20. E.J. Opila, R.C.; Robinson, and M.D. Cuy, “High Temperature Corrosion of Silicon Carbide and Silicon Nitride in Water Vapor,” in CIMTEC02, 2002, p. 14.

21. K.N. Lee, D.S. Fox, and N.P. Bansal, “Rare earth silicate environmental barrier coatings for SiC/SiC composites and Si_3N_4 ceramics,” J. Eur. Ceram. Soc., vol. 25, no. 10, pp. 1705–1715, 2005.
22. N.S. Jacobson, “Silica Activity Measurements in the Y_2O_3-SiO_2 System and Applications to Modeling of Coating Volatility,” J. Am. Ceram. Soc., vol. 97, no. 6, pp. 1959–1965, 2014.
23. G.C.C. Costa and N.S. Jacobson, “Mass spectrometric measurements of the silica activity in the Yb_2O_3-SiO_2 system and implications to assess the degradation of silicate-based coatings in combustion environments,” J. Eur. Ceram. Soc., vol. 35, no. 15, pp. 4259–4267, 2015.
24. S. Ueno, D.D. Jayaseelan, and T. Ohji, “Development of Oxide-Based EBC for Silicon Nitride,” Int. J. Appl. Ceram. Technol., vol. 1, no. 4, pp. 362–373, 2004.
25. R. Gonzalez-Julian, Jesus; Mauer, Georg; Sebold, Doris; Mack, Daniel; Vassen, “Cr2AlC MAX Phase as Bond-coat for Thermal Barrier Coatings: Processing, Testing under Thermal Gradient Loading and Future Challenges,” J. Am. Ceram. Soc., vol. in press, pp. 1–41, 2019.
26. D.S. Fox, R.A. Miller, D. Zhu, M. Perez, M.D. Cuy, and R.C. Robinson, “Mach 0.3 Burner Rig Facility at the NASA Glenn Materials Research Laboratory,” no. March, p. 34, 2011.
27. J.L. Smialek, “Unusual Oxidative Limitations for Al-MAX Phases. NASA/TM—2017-219444,” Cleveland, OH, 2017.
28. Z. Cheng et al., “Thermal Stability of YSZ Coatings Deposited by Plasma Spray–Physical Vapor Deposition,” Coatings, vol. 9, no. 8, p. 464, 2019.
29. J. Ilavsky and J.K. Stalick, “Phase composition and its changes during annealing of plasma-sprayed YSZ,” Surf. Coatings Technol., 2000.
30. H. Toraya, M. Yoshimura, and S. Somiya, “Calibration Curve for Quantitative Analysis of the Monoclinic-Tetragonal ZrO_2 System by X-Ray Diffraction,” J. Am. Ceram. Soc., 1984.
31. H. Toraya, “Effect of YO1.5 Dopant on Unit-Cell Parameters of ZrO_2 at Low Contents of YO1.5,” J. Am. Ceram. Soc., vol. 72, no. 4, pp. 662–664, 1989.
32. M.R. Gauna, M.S. Conconi, S. Gomez, G. Suárez, E.F. Aglietti, and N.M. Rendtorff, “Monoclinic-tetragonal zirconia quantification of commercial nanopowder mixtures by XRD and DTA,” Ceram. - Silikaty, 2015.
33. C.M. Ramos, A.S. Tabata, P.F. Cesar, J.H. Rubo, P.A. S. Fracisconi, and A.F. S. Borges, “Application of micro-raman spectroscopy to the study of yttria-stabilized tetragonal zirconia polycrystal (Y-TZP) phase transformation,” Appl. Spectrosc., vol. 69, no. 7, pp. 810–814, 2015.
34. R.A. Miller, J.L. Smialek, and R.G. Garlick, “Phase Stability in Plasma Sprayed Partially Stabilized Zirconia-Yttria,” in ADVANCES IN CERAMICS • VOLUME 3, SCIENCE AND TECHNOLOGY OF ZIRCONIA, 1981, pp. 242–253.
35. V. Lughi and D.R. Clarke, “Transformation of Electron-Beam Physical Vapor-Deposited 8 wt% Yttria-stabilized Zirconia Thermal Barrier Coatings,” J. Am. Ceram. Soc., vol. 88, no. 9, pp. 2552–2558, 2005.
36. J.L. Smialek, “Oxygen diffusivity in alumina scales grown on Al-MAX phases,” Corros. Sci., vol. 91, pp. 281–286, Feb. 2015.
37. J.L. Smialek, “Kinetic Aspects of Ti_2AlC MAX Phase Oxidation,” Oxid. Met., vol. 83, no. 3–4, 2015.
38. R.C. Robinson and J.L. Smialek, “SiC recession caused by SiO_2 Scale Volatility under Combustion Conditions: I. Experimental results and empirical model,” J. Am. Ceram. Soc., vol. 82, no. 7, 1999.
39. S. Mahade, N. Curry, S. Björklund, N. Markocsan, and S. Joshi, “Durability of Gadolinium Zirconate/YSZ Double-Layered Thermal Barrier Coatings under Different Thermal Cyclic Test Conditions,” Materials (Basel), vol. 12, p. 2228, 2019.
40. J.L. Smialek, “Oxidation of Al_2O_3 Scale-Forming MAX Phases in Turbine Environments,” Metall. Mater. Trans. A Phys. Metall. Mater. Sci., vol. 49, no. 3, pp. 782–792, 2018.

41. K. Lee, “Environmental Barrier Coatings Having a YSZ Top Coat,” ASME IGTI ; Pap. GT2002-30626, vol. 4, pp. 127–133, 2002.
42. D. Zhu, “Development of Advanced Environmental Barrier Coatings for SiC/SiC Composites at NASA GRC: Prime-Reliant Design and Durability Perspectives,” 2017.
43. K.N. Lee, “$Yb_2Si_2O_7$ Environmental barrier coatings with reduced bond coat oxidation rates via chemical modifications for long life,” J. Am. Ceram. Soc., vol. 102, no. 3, pp. 1507–1521, 2019.